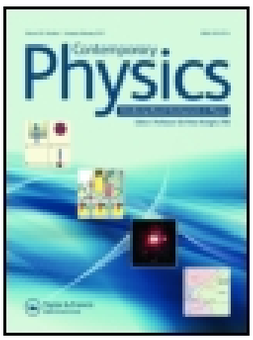

Contemporary Physics

ISSN: 0010-7514 (Print) 1366-5812 (Online) Journal homepage: http://www.tandfonline.com/loi/tcph20

Rayleigh-bénard convection

P. Bergé & M. Dubois

To cite this article: P. Bergé & M. Dubois (1984) Rayleigh-bénard convection, Contemporary Physics, 25:6, 535-582, DOI: 10.1080/00107518408210730

To link to this article: http://dx.doi.org/10.1080/00107518408210730

CONTEMP. PHYS., 1984, VOL. 25, NO. 6, 535–582

Rayleigh–Bénard Convection

P. Bergé and M. Dubois, Service de Physique du Solide et de Résonance Magnétique, CEN Saclay, 91191 Gif-sur-Yvette Cedex, France

ABSTRACT. This paper presents a physicist's approach to Rayleigh–Bénard convection widely illustrated with experimental results. The basis of the mechanism of the instability is simply presented with physical reasons for the existence of a critical threshold.

A detailed examination of the spatial organization is made with discussion of ordered and disordered structures. Furthermore it is shown that the measurements of the local velocity give a good quantitative description of the convective state.

A complete parallel between the Rayleigh–Bénard convection near onset and a critical phenomenon is given in the framework of a mean field approach, including both spatial as well as temporal effects. Non-Boussinesq convection is presented as symmetry breaking, changing the second order transition into a (partially) first order transition.

The last section is devoted to the ever present but still not completely understood question of the dynamics of the convective pattern; the importance of the existence and motion of defects is pointed out. Finally, a tentative and provisional survey is made of two open questions: the wavenumber selection and the approach of turbulence in large aspect ratio cells.

1. Introduction

Convection is a very common phenomenon in nature, and has fascinated many people for a very long time. Its study and understanding have fundamental importance in meteorology, oceanography, geophysics and astrophysics. Moreover thermal instabilities and related transport processes are involved in practical applications such as power engineering, combustion, material science, and space technology.

More precisely, phenomena as diverse as solar granulation, atmospheric structuring of planets, continental drift, striations in crystal growth, flame structure, atmospheric circulation etc.... are all related to thermal convection.

The origin of the term 'convection'—from the latin '*convectio*'—gives an idea of 'carrying with'. It seems to have been applied first to denote the transportation of heat through fluid motion. Thermal convection arises when a thermal inhomogeneity exists in a fluid. This thermal inhomogeneity is the source of motion through different mechanisms (such as surface tension etc....); but, on the other hand, stabilizing effects (such as viscosity) tend to dampen these motions. Then, generally, the competition between these two opposite effects leads to an instability. The fundamental characteristic of such instabilities is the existence of a threshold beyond which there is organization of motion into a relatively ordered pattern (J. Wesfreid *et al.* 1984).

This paper deals only with Rayleigh–Bénard convection which is one of the simplest instabilities. It corresponds to the case of a horizontal layer of a homogeneous, isotropic and dilatable fluid confined above and below by rigid plates of good thermal conductivity. (We shall not consider here non-Newtonian fluids, anisotropic fluids such as liquid crystals, mixtures of fluids or convection in porous media which could be a part of this field.) The fluid layer is submitted to a purely vertical adverse thermal gradient which, owing to buoyancy effects, will initiate destabilizing forces able to give rise to sustained motion.

Though evidences of convective motions had been pointed out by J. Thomson (1881–82), the first experimental and systematic work in the field of thermal convection was performed by H. Bénard (Bénard 1900) and the first theoretical approach was

made by Lord Rayleigh (Rayleigh 1916), hence the name 'Rayleigh–Bénard convection'.

In fact, Rayleigh established the theory of buoyancy driven convection in order to explain, in particular, Bénard's observations. We now know that the theory was not in fact relevant in this particular case: Bénard was studying convection in a shallow oil layer with an upper free surface for which the surface tension effects are dominant.

In the case of the 'pure' Rayleigh–Bénard convection, the field of investigation is so broad that it is very difficult to consider making an exhaustive review, even if only the recent studies are considered. Because of this, we have preferred to choose illustrations which were principally obtained in our laboratory.

2. Mechanism of the instability

2.1. *Basic processes and characteristic times*

Consider a horizontal layer of isotropic fluid—water for example—which is confined between two horizontal plates of good thermal conductivity to provide perfect isotherms at the boundaries. If we apply, during a sufficiently long time, a temperature difference ΔT such that the lower plate is the colder, the heat flux ϕ which crosses the fluid establishes a linear profile of temperature in the layer. See Figure 1 (*a*). The heat flux which is necessary to maintain this constant gradient is

$$\phi = \left(\frac{\Delta T}{d}\right) S \Lambda_T \tag{1}$$

Λ_T being the thermal conductivity of the fluid, S the surface area of each plate and d the distance between the two plates.

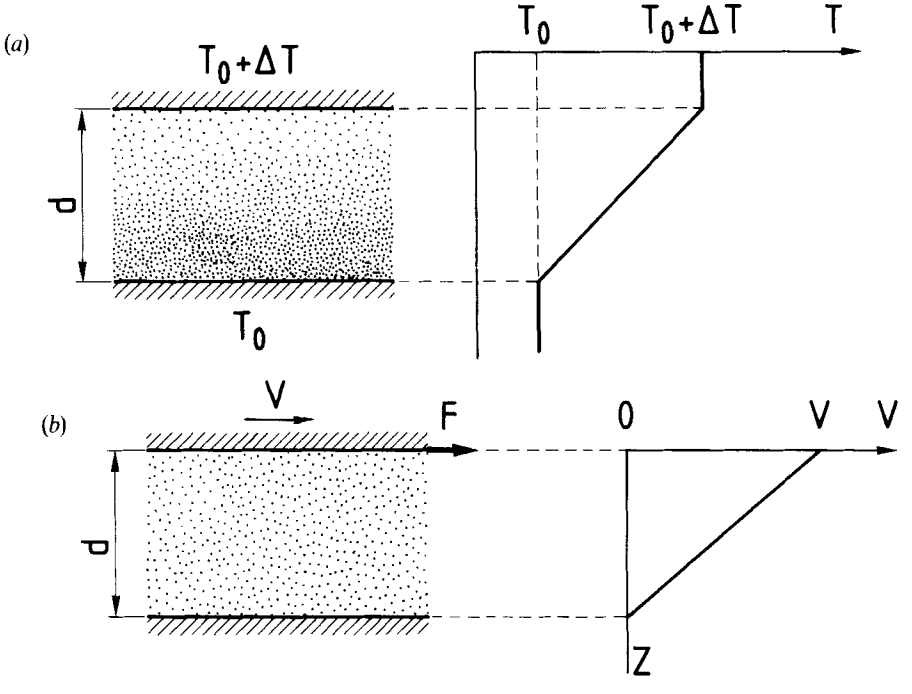

Figure 1. (*a*) Asymptotic linear temperature profile in a fluid layer submitted to a stabilizing temperature gradient. (*b*) Asymptotic velocity profile in a fluid layer submitted to a shear produced by the translation with velocity V of the upper plate.

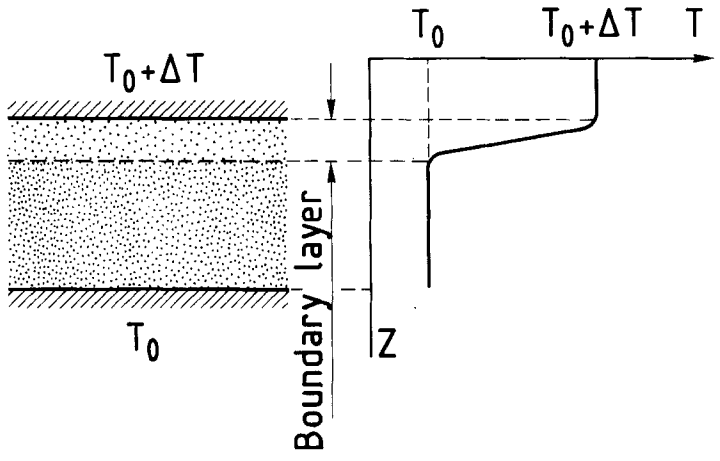

Figure 2. Transitory temperature profile following a sudden change of the temperature at one horizontal plate: formation of a transitory boundary layer.

In the same manner, if we apply a velocity difference between the top and the bottom of the layer (supposed here to be at the same temperature) a linear profile of velocity is established after a given time (this may be obtained by a translation of the top plate in its plane see figure 1 (*b*)). The force F required to be applied to the top plate with surface area S in order to shear the fluid and to maintain constant the velocity gradient is

$$F=\frac{dV}{dZ}S\eta \tag{2}$$

where η is the dynamical viscosity of the fluid.

In the stationary regime, since $dV/dZ=V/d$,

$$F=\frac{V}{d}S\eta \tag{3}$$

On the other hand, suppose now that we suddenly apply the temperature difference ΔT (or the velocity difference V) to the layer. At the beginning, only a thin fluid layer will be heated (or sheared) in the vicinity of the plate that has been suddenly heated (or translated): a boundary layer has been formed, inside which the entire temperature (or velocity) gradient is localized (see figure 2).

The propagation of these localized gradients through the whole fluid layer is governed by a diffusion equation. The diffusion coefficient of the temperature is

$$D_T=\frac{\Lambda_T}{\rho_0 C_p} \tag{4}$$

where C_p is the specific heat at constant pressure and ρ_0 the density. The diffusion coefficient of the velocity gradient (more generally of the vorticity) is simply the kinematic viscosity $\nu=\eta/\rho_0$.

These coefficients allow us to calculate the order of magnitude of the characteristic relaxation times τ of the gradients in the layer of depth d. For the temperature:

$$\tau_{th}\simeq d^2/D_T, \tag{5}$$

and for the velocity:

$$\tau_v \simeq d^2/v. \tag{6}$$

The ratio of these times is the Prandtl number which controls the temporal behaviour in a fluid layer submitted to the two kinds of gradient. Then in convective motion,

$$Pr = \frac{\tau_{th}}{\tau_v} = \frac{v}{D_T} \tag{7}$$

We may have two opposite situations:

(*a*) High Prandtl number fluids: the vorticity diffuses (then the velocity relaxes) faster than the temperature. Then the velocity perturbations follow the temperature perturbations without delay; one says that the viscous effects are dominant.

(*b*) Low Prandtl number fluids: the temperature relaxes faster than the vorticity: a velocity perturbation may persist even after the thermal cause has disappeared: the inertial effects are dominant.

From these two opposite situations, one can point out the qualitative analogy between the Prandtl number and the reciprocal of the Reynolds number *Re*, because, in a flowing liquid, *Re* measures the balance between inertial terms and viscous terms.

2.2. *Test of the stability of the layer*

We consider now the case in which the lower plate is warmer than the top plate and we are at equilibrium, i.e. a constant temperature gradient is established in the layer.

At first sight, it would seem that the stratification formed by denser layers located above less dense layers is necessarily unstable. Let us show that this is not true. In fact we must point out that a fluid element such as B in figure 3, which is located in the less dense region, is *not* subjected to any force tending to push it upwards, since its horizontal surroundings are of the same density. On the contrary, let us see what happens if we initiate the motion of B by a small displacement towards B′. If this

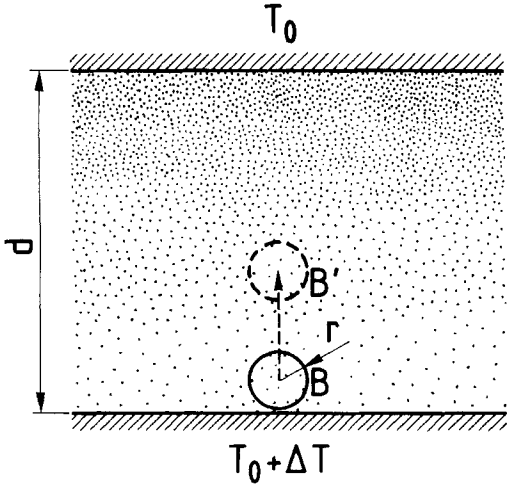

Figure 3. Displacement of a spherical fluid element in order to examine the different forces acting on this element after an initial ascending motion.

displacement has been sufficiently rapid so that the temperature relaxation of the element is negligible, then this element will be surrounded by denser regions producing an archimedean force. This force may sustain the initial ascending displacement. The fundamental question about the stability of the layer can be summarized in the following question: during the time required for the fluid element to move a distance of order of magnitude d, has the thermal diffusivity relaxed the temperature difference between the fluid element and its new surroundings? (Note that this temperature difference is necessary in order to have a buoyancy maintaining the motion). So we must compare two times: the advection time and the time of thermal relaxation. Let us take a purely dimensional approach. After the initial displacement the fluid element is subjected to two opposite forces. The first is the archimedean buoyancy force F_A which is proportional to the acceleration of gravity g, to the fluid density ρ_0, to the volume expansion coefficient α, to the temperature difference ΔT and to the volume of the element r^3:

$$F_A \sim g\alpha\rho_0 \Delta T r^3 \tag{8}$$

Secondly we have the viscous force F_V whose direction is opposite to that of the motion. From the Stokes formula, this force is given by

$$F_V \sim 6\pi\eta r V \tag{9}$$

where η is the dynamical viscosity and V the velocity of the fluid element (we suppose here that the element is a sphere of radius r). V is determined by equalizing F_A and F_V. Then we can calculate the time taken by the element to move along d:

$$t = \frac{d}{V} \simeq \frac{6\pi d\eta}{g\alpha\rho_0 \Delta T r^2} \tag{10}$$

The motion will be sustained if the thermal relaxation time is greater than t, $\tau_{th} > t$ i.e. $d^2/D_T > 6\pi d\eta / g\rho_0 \alpha \Delta T r^2$.

It is clear that large fluid elements are favoured in their motion (high velocity and long thermal life time). So if we consider elements whose radius is, in the limit, of the order of d, the condition of motion, and thus of instability, can be written:

$$\frac{\rho_0 \alpha g \Delta T d^3}{\eta D_T} > A \tag{11}$$

or, since $\nu = \eta/\rho_0$

$$\frac{g\alpha\Delta T d^3}{\nu D_T} > A \tag{12}$$

where A is a constant.

The expression on the left is called the Rayleigh number Ra. It is the dimensionless parameter which governs the stability of a fluid layer subjected to a destabilizing vertical thermal gradient.

Then, if Ra is higher than a certain value A, the motion of the layer will begin.

This phenomenological approach has the advantage of showing clearly the different mechanisms which intervene in the thermal convection without involving the

details of the theoretical formulation of the problem. In fact, the full set of equations describing the system exactly is formed by

— the equation of state $\rho = \rho_0(1 - \alpha T)$ (13)
—the Navier–Stokes equation
— the heat or energy equation
—and the continuity equation which accounts for the mass flux conservation and which, for a fluid of nearly constant density, is written

$$\operatorname{div} \mathbf{V} = 0 \tag{14}$$

From this set of equations and the boundary conditions considered above one can calculate the exact critical value Ra_c beyond which convective motions set in. This universal value, independent of the fluid, is $Ra_c = 1707$. This value is valid in the case of infinite geometry (great horizontal extent of the layer compared to d) and very good conductivity of the horizontal plates (Normand *et al.* 1977).

Some critical temperature differences, corresponding to Ra_c, are reported in the following table which gives the threshold of the motion for some fluids near room temperature (and $d = 1$ cm).

	air	water	Si oil $\nu = 1$ stokes
ΔT_c ($d = 1$ cm)	17°	0·1°	2·2°
Pr	0·7	7	900

Table 1. Some critical temperature differences corresponding to Ra_c for some fluids near room temperature.

When the horizontal extension is finite in comparison with the depth (in fact when it is between one and a few times the depth), the Ra value corresponding to the threshold of the motion becomes progressively higher than 1707, as the extension becomes lower; this increase is due to the stabilizing effects of the lateral boundaries. (Stork and Müller 1972).

2.3. *Bifurcation. Onset of the instability*

Let us return to the model of the spherical fluid element discussed previously. For reasons of symmetry, downwards motion of the denser element has the same probability of occurring as the upwards motion of the less dense element; indeed, at the same place, one of the possibilities excludes the other (see figure 4(*a*)). When convective motion sets in, a choice must be made for the velocity direction at a given point in the layer. This equiprobability may be shown schematically as in figure 4(*b*): at Ra_c there is a bifurcation to two symmetrical branches. On the other hand the stability of the quiescent state has been exchanged with that of the convective state: we say that we have an exchange of stabilities at Ra_c. These properties of symmetry and bifurcation are to be contrasted with what happens when the temperature gradient is horizontal instead of vertical (figure 5). In this case, the configuration is immediately unstable: it is not necessary to shift the fluid element to test its stability. Any hot element always has denser fluid in its horizontal environment and therefore moves immediately upwards while any cold element descends, no matter how small the temperature difference.

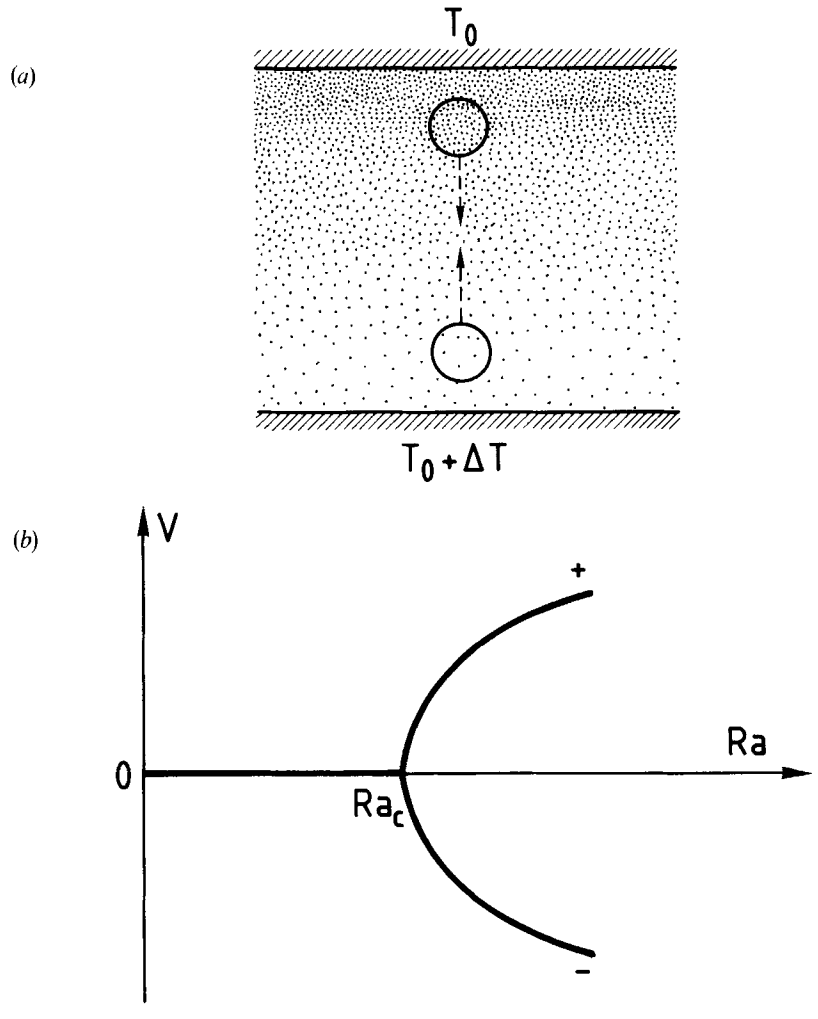

Figure 4. (*a*) Illustration of the competition between ascending motion of a hot element and descending motion of a cold element. (*b*) Illustration of a normal bifurcation at Ra_c between the steady state ($Ra < Ra_c$) and the convective states.

There is no threshold for thermoconvection due to horizontal temperature gradients. Correspondingly, the ambiguity in the direction of the velocity (downwards or upwards) does not exist: there is necessarily ascending motion at the hot plate and descending motion at the cold plate.

In the case of the Rayleigh–Bénard configuration, the choice between one branch of the bifurcation or the other is completely arbitrary only in an experiment exempt from defects. In practice the smallest imperfection, such as the presence of a horizontal gradient at a lateral wall confining the layer, removes the degeneracy. We can use that to select the sign of the velocity at the lateral boundaries, for example by playing with the experimental situation in crossing $\Delta T = \Delta T_c$. Generally the lateral boundaries confining the fluid, of plexiglass for example, have a higher thermal diffusivity than that of the fluid. So, if we exceed ΔT_c (from a ΔT just below ΔT_c) by a relatively fast heating at the bottom plate, the heat diffuses faster in the lateral boundaries which are, then,

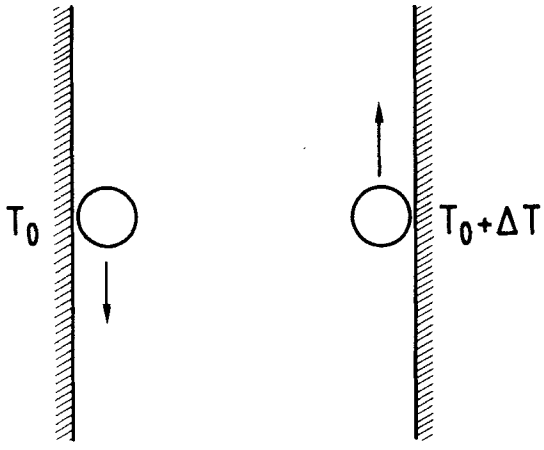

Figure 5. Fluid layer submitted to a horizontal thermal gradient.

temporarily warmer than the fluid; the induced horizontal gradient favours an ascending motion at this boundary which determines the choice of one branch of the bifurcation.

If, on the contrary, we cool the top plate, we can see by a similar argument that the convection starts with descending motion at the lateral boundaries.

All that has been said above holds only at the onset of convection: the structure may evolve further as we will see in the following. Nevertheless it is very important to point out at the outset the essential role played by the conditions at the lateral boundaries at the beginning of convection.

Let us mention another kind of perturbation which may exist at the lateral boundaries in a permanent way. This is the case when the thermal coupling between the isothermal horizontal boundaries and the lateral ones is not the same below and above. Let us suppose for example a better thermal contact with the bottom plate (see figure 6). The temperature of this lateral wall will be then slightly higher than in the fluid, producing a permanent uprising current at this boundary (even below the onset of Rayleigh–Bénard convection). We will see later that this perturbation may completely inhibit the occurrence of the preferred convective structure.

Finally let us mention a case in which, in the absence of any thermal imperfection of the cell, the equiprobability and symmetry of uprising and down going fluid is broken. Up to now we have supposed that the physical properties of the fluid which are involved in the Rayleigh number are temperature independent (except, of course for the density!): this is the so called Boussinesq approximation. In contrast we now assume that one of these physical properties varies substantially with temperature so that its value is significantly different near the cold plate compared with near the warm plate (non-Boussinesq fluid). For example if the viscosity is noticeably higher near the cold plate than near the warm plate the warm fluid then has a Rayleigh number which is higher than that of the cold fluid and a reasoning similar to that given above (see figure 4(*a*)) shows that while a small displacement of a hot sphere will sustain motion, the same operation made with a cold sphere will *not* be so effective, and it may even be without effect. Clearly uprising motion will be favoured, downgoing streams existing simply to ensure conservation of the flux (see figure 7). In the example considered here, the driving force of the convection being (mainly) located at the bottom, the velocity

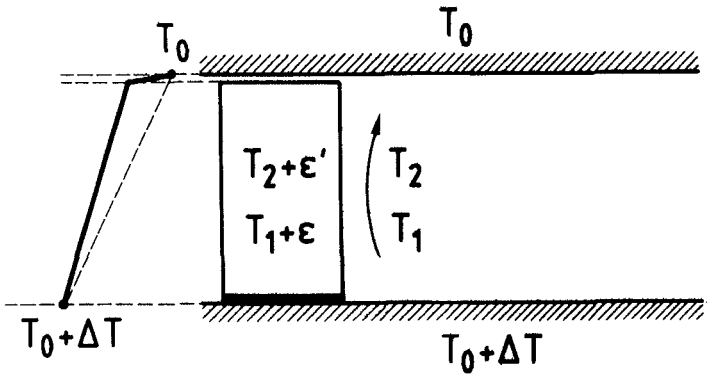

Figure 6. Dissymmetry of the thermal coupling of a lateral boundary with the top and the bottom plates. Here the coupling is imperfect at the top plate producing a breaking in the thermal profile as shown at the left of the figure (full line, profile in the boundary; dashed line, profile in the layer). The resulting horizontal gradient produces a permanent uprising motion at the boundary.

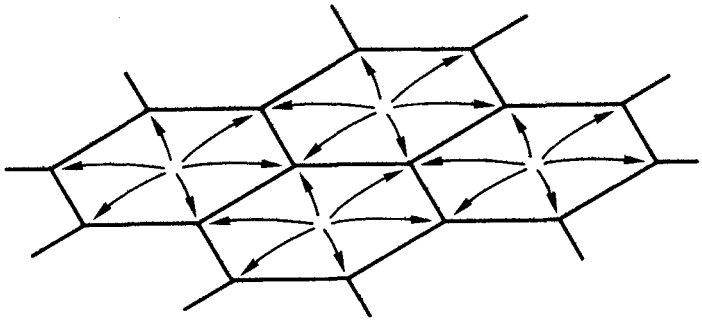

Figure 7. Scheme of a cellular hexagonal pattern with an uprising motion at the centre of the hexagons.

amplitude of upgoing streams will be higher than that of the downgoing streams†. The situation depicted here contrasts strongly with the case of Boussinesq convection studied up to now: the structure with rolls is no longer compatible with the asymmetry in the amplitudes of the up and down velocities and the bifurcation is no longer normal. We shall see later that this non-Boussinesq convection implies a new kind of structure, i.e. the hexagonal pattern; here, and in contrast with what happens with rolls, the sign of the velocity in the centre of the hexagons is determined, *a priori*, by the nature of the non Boussinesq effect.

The same kind of asymmetry in the motion also occurs in the case of Bénard–Marangoni convection, i.e. with a free surface at the top of the fluid. In this case, the active force is given by the thermal variation of the surface tension and is only present in the upper part of the fluid. In this case, an hexagonal pattern is also formed (see figure 8) as pointed out by the pioneering work of Bénard (Bénard 1900).

† The reverse will be true if, for example, the viscosity were higher at the hot plate which is the case for gases: here, downward velocity amplitude will be higher.

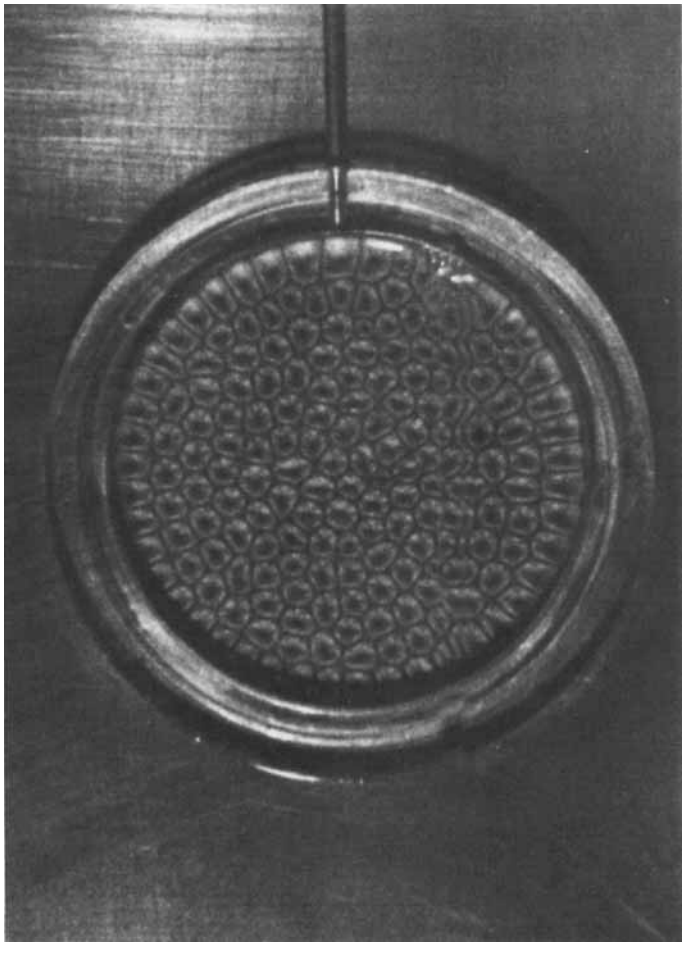

Figure 8. Photograph of a cellular pattern observed with a shallow layer of silicone oil heated from below and with a free surface at the top. Visualization is achieved through aluminium powder suspended in the oil. Note many imperfections in the hexagonal arrangement.

3. Spatial organization

3.1. *Natural structures*

We have seen that when the temperature difference applied to a horizontal fluid layer is increased beyond a given value (or $Ra > Ra_c$), the fluid begins to move. How does it do this?

To study this, it is necessary to look at the fluid from above. This is the reason why, in experiments which deal with this problem, the upper plate is often made of transparent sapphire whose thermal conductivity is large compared to that of the usual fluids. Furthermore, up to now, the major part of the observations has been performed with high Prandtl number fluids ($Pr > 1$) near room temperature. Then it is easy to see just by looking with the naked eye at dust particles suspended in the fluid that a 'dynamical' structure takes shape: there is an organization of ascending and descending motions which carry along the fluid, in rolls turning clockwise or counter-clockwise successively in space (see figure 9). These particular motions obviously introduce in the

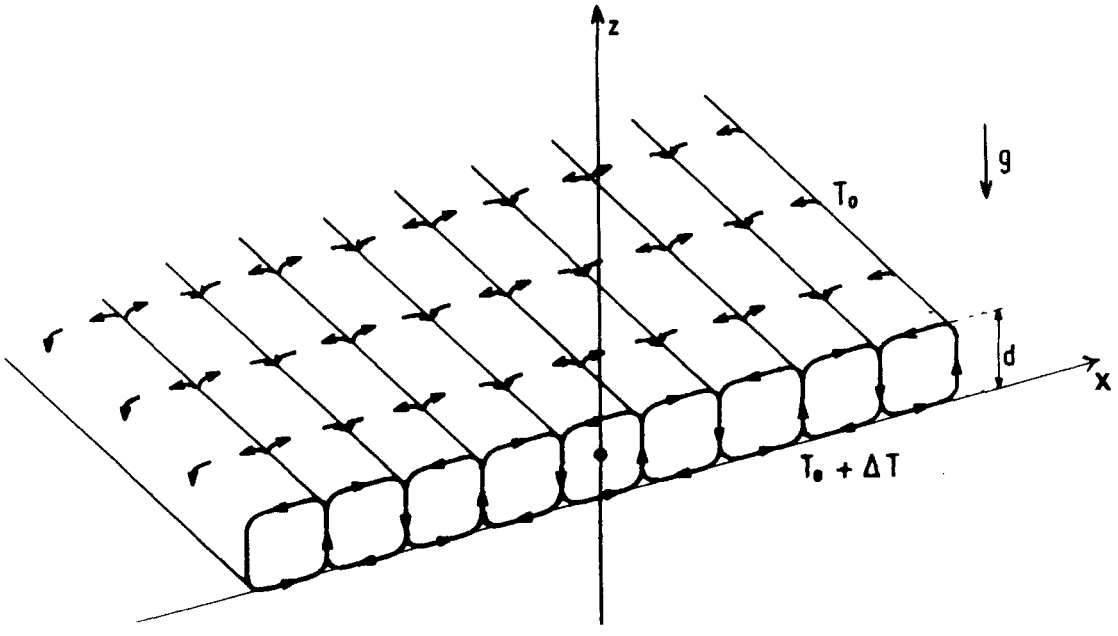

Figure 9. Schematic diagram of the organization of convective motions into rolls.

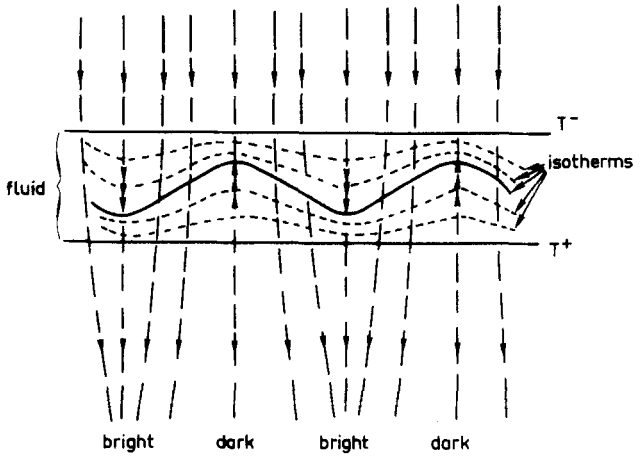

Figure 10. Principle of the visualization of the convective pattern through the focusing effect, due to thermal gradients ('Shadowgraphic' method).

fluid a succession of 'warm' and 'cold' currents. One can make these currents visible (without perturbing the fluid) through the temperature gradients which induce refractive index gradients able to refract light beams (see figure 10) so that the fluid acts as many local lenses. Then, a parallel light beam which crosses the fluid is focused where the refractive index is largest (cold streams) and diverges where the refractive index is lowest (warm streams): the light intensity modulation of the beam after crossing the convective cell reveals the structure of the motion (see figure 11) with bright lines corresponding to downwards motions. All the patterns, shown in the following are obtained with this technique.

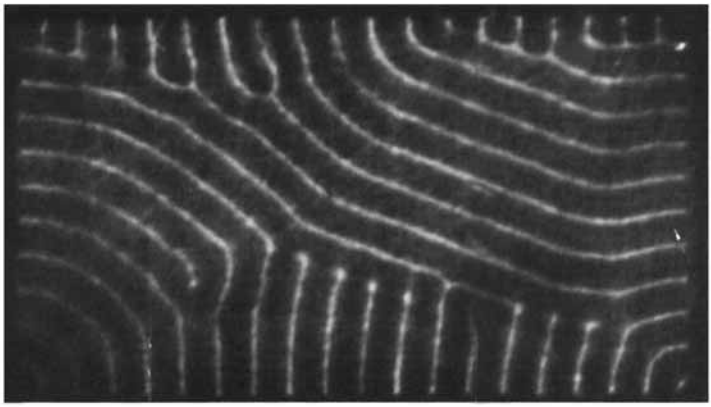

(a)

(b)

Figure 11. Typical disordered structures near the onset of Rayleigh–Bénard convection. (Silicone oil, $\nu = 0{\cdot}05$ stokes). (*a*) rectangular container $\Gamma_x = 38$, $\Gamma_y = 24$. (*b*) cylindrical container $\Gamma = 20$.

If the horizontal extent of the layer is large compared to the depth d, we generally obtain (after a transient period which may be very long) a stationary (time-independent) roll pattern which has the following properties:

(*a*) the axes of the rolls tend to be perpendicular to the lateral walls.
(*b*) In the core of the pattern, relatively far from the boundaries, the axes of the rolls are equidistant and so locally parallel.

These two properties are independent of the form of the frame which confines the fluid layer horizontally (e.g. rectangular, circular etc.). (Bergé 1981, Gollub *et al.* 1982 a, Stork and Müller 1975). Except for some particular cases, these two conditions cannot be simultaneously fulfilled, creating a topological frustration. This frustration gives rise to defects such as dislocations, bending of the rolls, grain boundaries... See figure 11. (Croquette *et al.* 1983). Another peculiarity of the motion is that, near onset, the motion

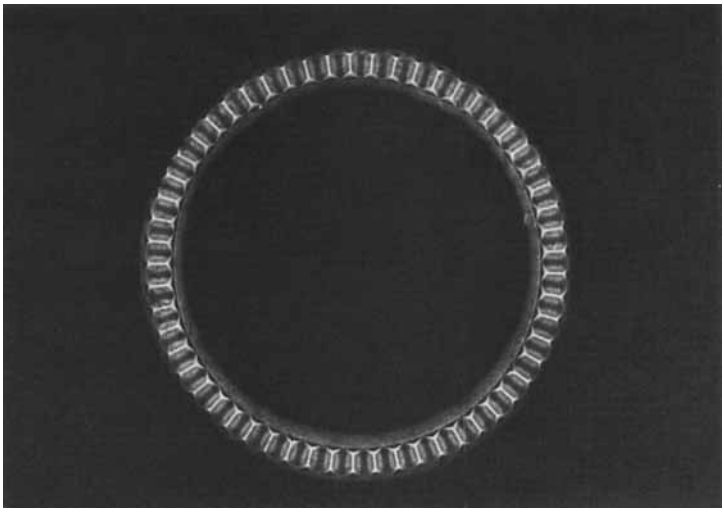

Figure 12. Ordered pattern of radial rolls in an annular container. The ratio of the gap to the depth is 2,3. (Silicone oil, 0·05 stokes).

is to a first approximation two-dimensional: if we follow the motion of a small dust particle carried by the convective fluid we notice that its trajectory lies in a vertical plane.

3.2. *Ordered structures*

We have seen an important property of the convective motion near onset, i.e., its remarkable collective organization, but with breakdown of the spatial order at large scale because of the presence of defects. Nevertheless, we can obtain quasi-perfect structures with long range order by imposing some constraints.

These constraints may be geometrical. Knowing the very important role played by the lateral boundaries, the spatial properties of the motion depend on the extent of the layer. We must therefore define a new parameter, the aspect ratio Γ which is the ratio of a horizontal dimension to the depth. In the case of a cylindrical cell, $\Gamma = R_d/d$ where R_d is the radius. For a rectangular frame, the geometry is defined by two aspect ratios $\Gamma_x = L_x/d$ (L_x is generally the greater length) and $\Gamma_y = L_y/d$. If Γ_y is of the order of d ($1 < \Gamma_y < 3$ to 5), the geometrical constraint induces a given orientation for the roll axes such as to make them perpendicular to the larger side of the cell. The same idea holds in an annular frame where the fluid layer is confined between two cylinders, when the gap between them is small and the radius of curvature large compared to d. (See figure 12.)

Alternatively, one can impose local thermal constraints. If we heat the fluid locally, for example with a powerful light beam, one induces ascending motion in the illuminated area which will initiate local uprising streams. This may stabilize certain structures (see figure 13). In this way a structure with concentric rolls may be obtained in a cylindrical cell by a small heating at the ring boundary (see figure 14); the pattern would otherwise be as shown in figure 11. This method of local heating may also be used to induce various structures (within certain limits obviously) whose spatial and dynamical properties can be studied by the physicist (Chen and Whitehead 1968). To do this, the fluid just below ΔT_c is heated locally according to a chosen pattern (see figure 15). Then ΔT is increased beyond ΔT_c and the local heating is suppressed allowing the convection to evolve from the imposed pattern.

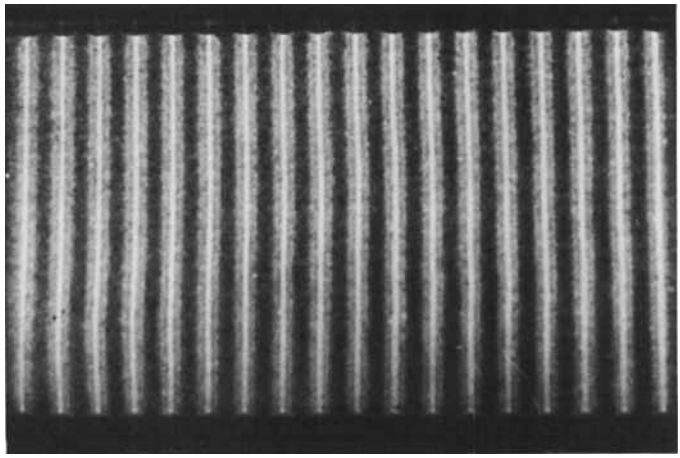

Figure 13. Ordered pattern of straight rolls in a rectangular container $\Gamma_x = 38$, $\Gamma_y = 24$. (Silicone oil 0·05 stokes). In spite of the large aspect ratios Γ_x and Γ_y, an ordered structure is stabilized by the presence of a small horizontal thermal gradient, purposely created along the two shorter sides of the frame.

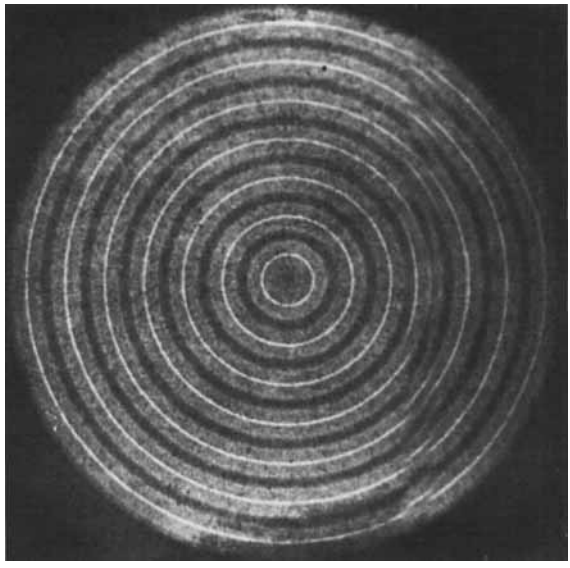

Figure 14. Ordered pattern of concentric rolls forced by permanent heating at the cylindrical boundary ($\Gamma = 20$, Silicone oil 0·05 stokes).

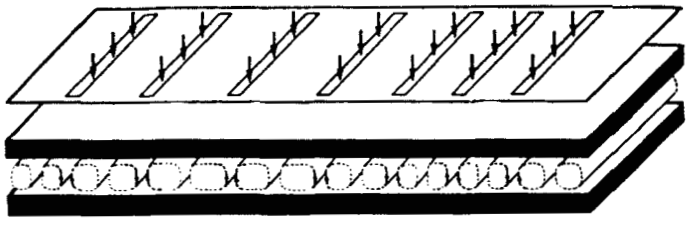

Figure 15. Sketch of the experimental set up for structure induction; the arrows stand for the powerful light illumination. The perforated mask above the cell reproduces the desired pattern; (here the mask will give a phase modulation corresponding to a longitudinal mode).

We must also note the influence of hydrodynamical constraints: if the convective fluid layer is submitted to a mean flow in a horizontal direction, the roll axes tend to be aligned along the external flow direction. If the mean flow is vertical, the geometry of the pattern depends on this flow: a cellular (hexagonal) pattern is stabilized when this flow has large amplitude, whereas rolls are stable for small amplitude of flow. An interesting study of this phenomenon has been made by R. Krishamurti (1975), in relation to the formation of cloud patterns.

3.3. *Velocity field in the case of bidimensional rolls*

Until now, we have spoken of the global spatial organization. To understand more quantitatively the spatial properties, we look now at the velocity field as it has been measured, point by point, by laser Doppler anemometry, in a quasiperfect structure (Bergé and Dubois 1981). The examples we give later have been performed in rectangular cells with aspect ratios $\Gamma_x = 10$, $\Gamma_y = 3$ and $\Gamma_x = 30$, $\Gamma_y = 6$ where the rolls, parallel to the short side of the cell, are therefore two-dimensional (as shown in figure 13).

The precise study of the velocity field along a pair of rolls shows that we have effectively a sinusoidal mode, the two components of the velocity, V_z and V_x (V_z: vertical and V_x: horizontal) varying as:

$$V_z = {}^{\circ}V_z(z)\cos(ax+\varphi) \tag{15}$$

$$V_x = {}^{\circ}V_x(z)\sin(ax+\varphi) \tag{16}$$

(see figure 16), a is the wavenumber $= 2\pi d/\Lambda$ with Λ the wavelength i.e. the distance between two ascending or descending motions. φ is the phase which defines the position of the rolls. The continuity equation $\operatorname{div}\mathbf{V} = 0$, implies that the two components V_z and V_x are phase-shifted by $\pi/2$.

The z-dependence $V_z(z)$ and $V_x(z)$ is determined by the horizontal boundary conditions at the top and bottom plates, which in the rigid-rigid case are:

$$V_x = V_z = 0 \quad \text{and} \quad \frac{\partial V_z}{\partial z} = \frac{\partial^2 V_z}{\partial z^2} = 0.$$

In the unrealistic case of free-free boundaries, the z dependence would be sinusoidal; in the rigid-rigid case, it is a sum of hyperbolic functions; note only that ${}^{\circ}V_z$ is maximum in the midplan of the layer $z = d/2$, and that ${}^{\circ}V_x$ is maximum at two levels $z \simeq 0{\cdot}22d$ and $z \simeq 0{\cdot}78d$, as can be seen on figure 16 (*b*) which shows the measured dependence $V_x(z)$. There is good agreement between the experimental profile and the calculated one (Bergé 1976; Normand *et al.* 1977). Note the symmetry between the velocity fields away from the plane $z = d/2$ which imposes $V_x \equiv 0$ in the mid-plane of the layer. In each point of the fluid, the velocity $\mathbf{V}$ is given by the combination of V_x and V_z. The streamlines, which are tangent at any point to $\mathbf{V}$, are closed loops inside each roll, as shown in figure 17 where parts of the trajectories of dust particles versus time have been followed. The boundary between two rolls is a vertical plane.

If the velocity field is measured in the entire layer, we notice the similarity of the velocity amplitude from one roll to another, as shown in figure 18 supporting the previous assumption of the presence of a well defined spatial mode.

Nevertheless, when the Rayleigh number is increased, the study of the velocity field (always in the approximation of two-dimensional motion) reveals unambiguously the presence of second and third spatial harmonic modes, brought about by the increasing

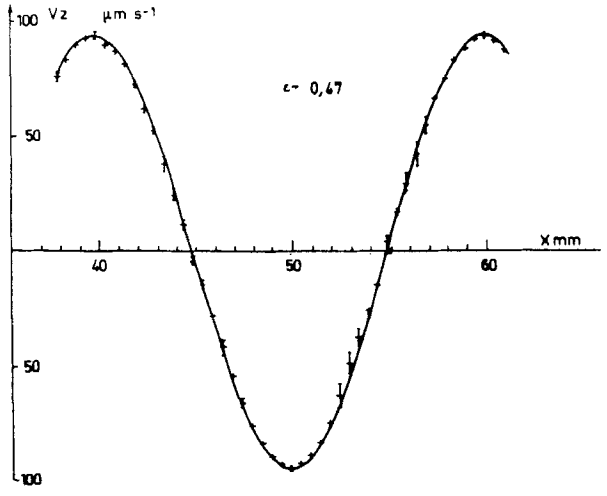

(*a*)

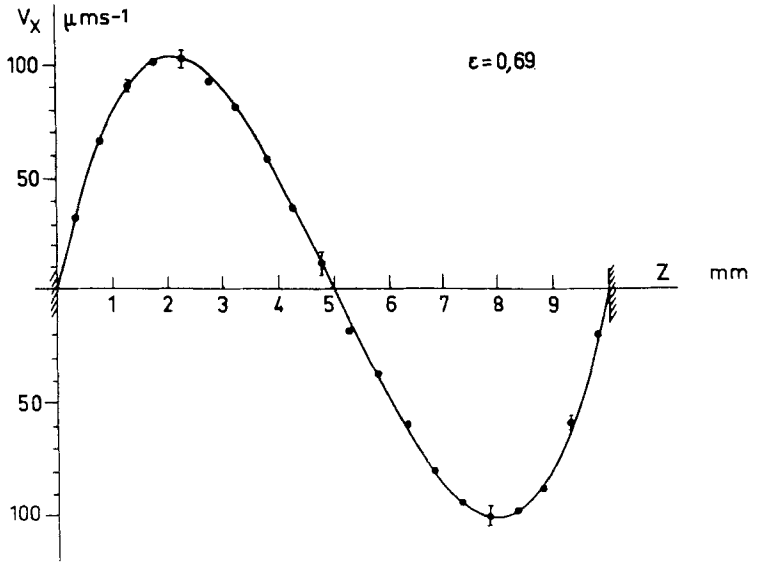

(*b*)

Figure 16. Velocity profiles determined by laser Doppler anemometry (Silicone oil, $Pr \simeq 900$, $d = 1$ cm, $\Gamma_x = 10$, $\Gamma_y = 3$). (*a*) Vertical component of the velocity V_z measured at the mid height plane as a function of x. (*b*) Horizontal component of the velocity V_x as a function of z. V_x is measured along the vertical axis passing through the centre of a roll.

influence of the non-linear terms. The spatial properties of these harmonic modes are in agreement with calculations (Dubois *et al.* 1978). The main features are shown in figure 19; the second harmonic may be represented by four rolls, the third harmonic by three elongated rolls inscribed in the fundamental roll. The motion is then due to the superposition of the fundamental mode and of the harmonics.

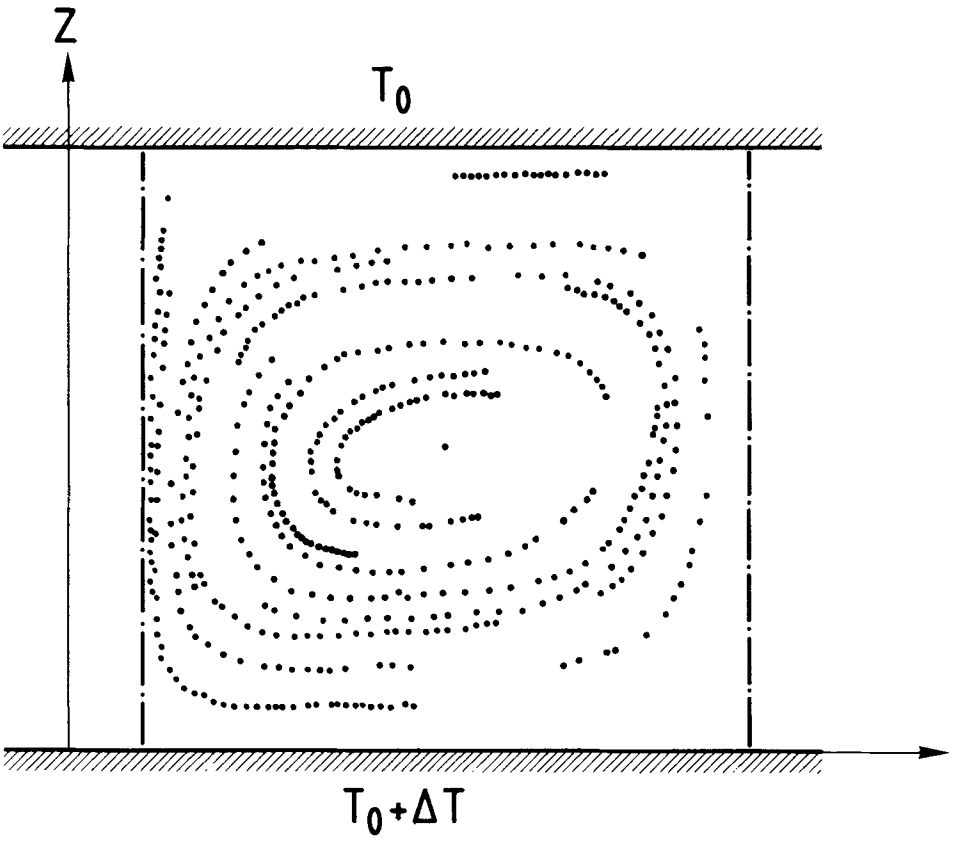

Figure 17. Successive positions of dust particles suspended in a convecting fluid drawn from a movie, image by image. Each dot represents a particle at a given instant. Note that the trajectories at the boundary of the roll are vertical lines. ($\varepsilon \simeq 2$).

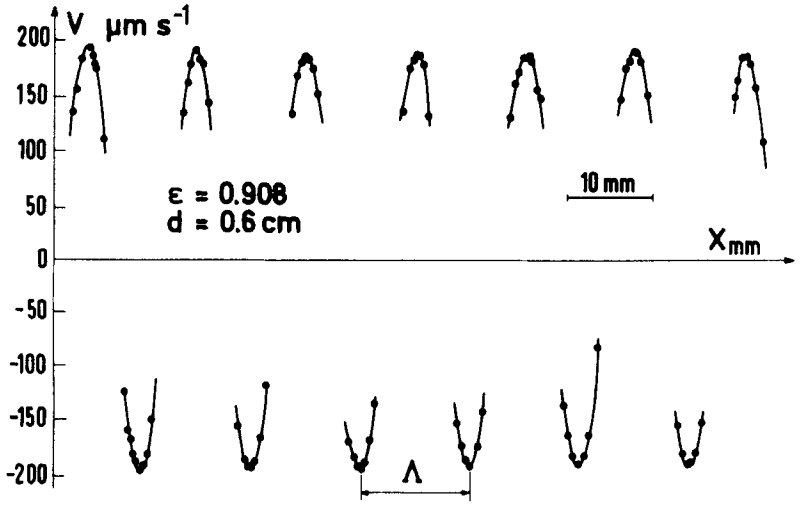

Figure 18. Horizontal component of the velocity versus x measured along 13 rolls.

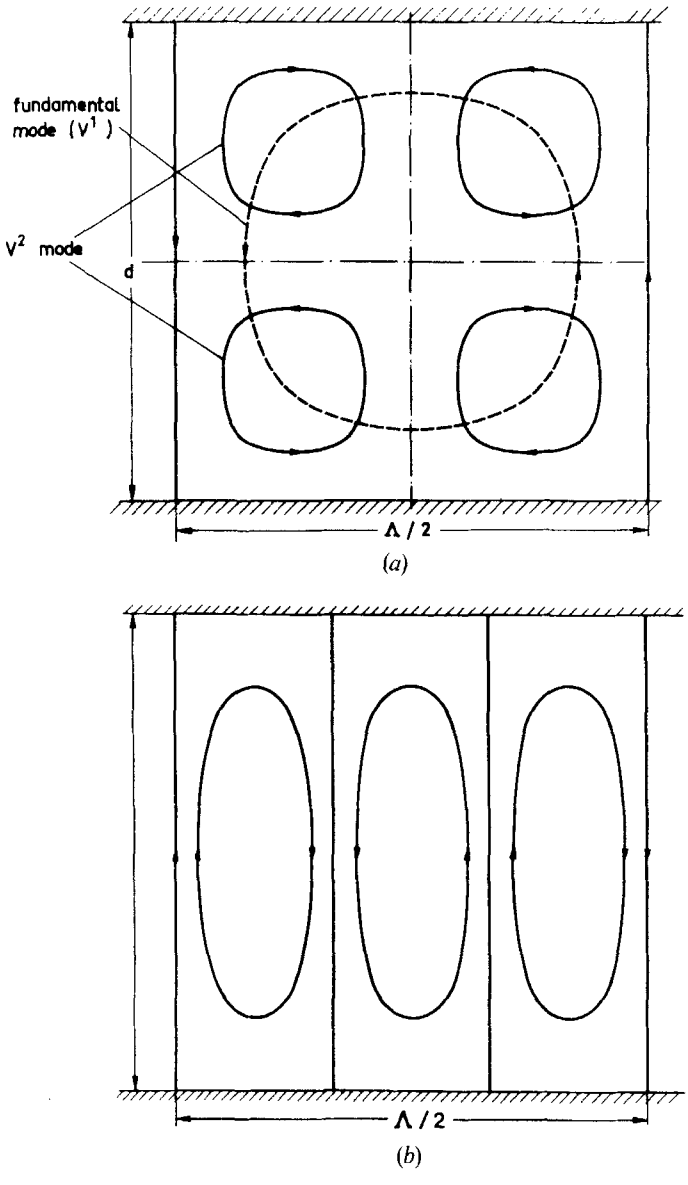

Figure 19. Schematic representation of the spatial properties of the harmonic modes. (*a*) Second harmonic mode (of wavelength Λ/2). (*b*) Third harmonic mode (of wavelength Λ/3).

3.4. *Heat transport—temperature profile*

When the velocity is zero (*Ra* just below Ra_c) the heat flux through the layer is carried only by conduction of the fluid, and the isothermal lines are horizontal and equidistant.

When convective motions are present, the heat flux is carried by conduction *and* by (vertical) convection. Vertical uprising streams such as BB′, are warmer than the mean temperature whereas descending motions like AA′ are colder (see figures 20(*a*) and 20(*b*)) (at 0, the centre of the roll, the temperature is not perturbed owing to the absence of motion). These motions produce a distortion of the isothermal lines which are either pinched or dilated in the region of the vertical streams. One can see in figure 20(*c*), a

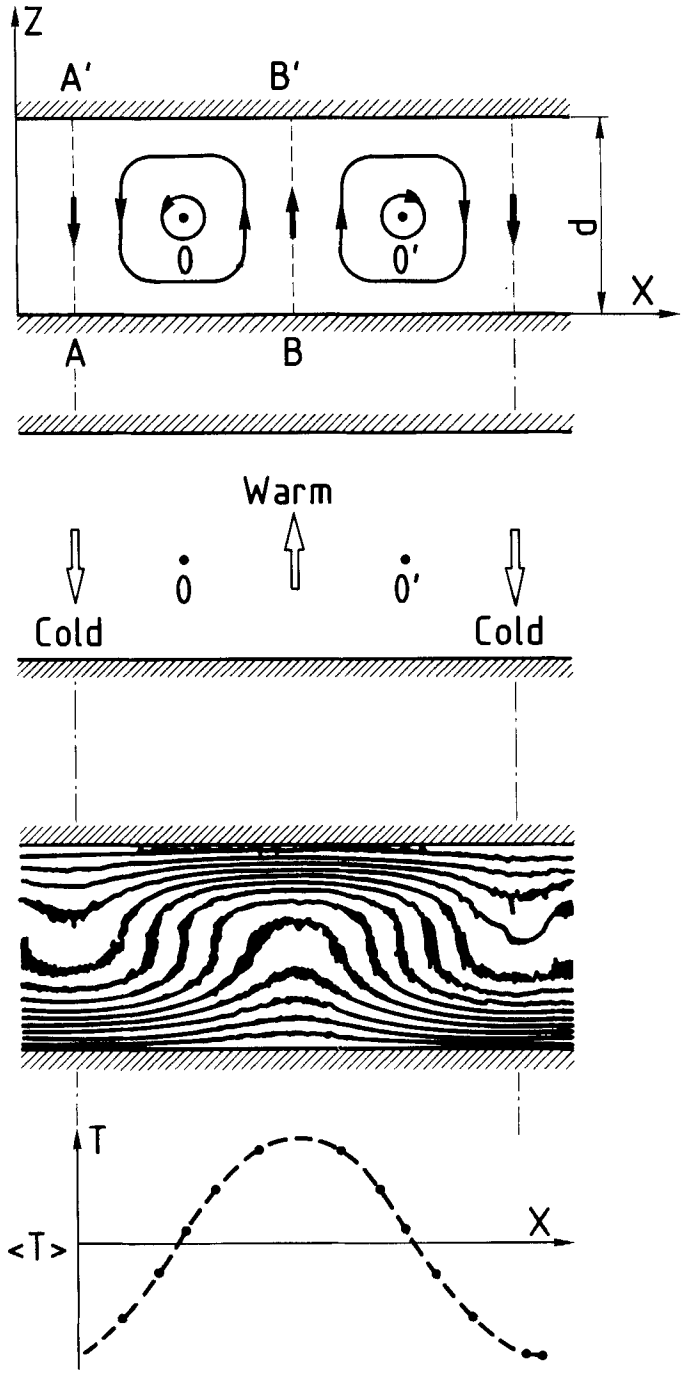

Figure 20. Relation between the velocity field and the local temperature of the fluid. (*a*) Schematic diagram of the stream lines. (*b*) Maximum vertical streams. (*c*) Interference fringes with represent isotherm lines in a vertical plane. (Water, $\varepsilon = 1{\cdot}2$, from R. Farhadieh *et al.* 1974.) (*d*) Temperature profile in the mid height plane of the layer as deduced from (*c*).

representation of such isothermal lines measured in a layer of convecting water using interferometric techniques (Farhadieh and Tankin 1974). From these isothermal lines one can deduce the temperature at any point of the layer, for example in the mid height plane; the result is shown in figure 20(*d*) and one can see, as also for the velocity, that near the onset of convection, the temperature variation versus x is sinusoidal around the mean temperature of the layer $\langle T\rangle = T_0 + \Delta T/2$ (see also Bühler *et al.* 1979).

One can clearly see in figure 20(*c*) that the isotherms are closely spaced (large thermal gradients) near the horizontal boundaries, this effect being more and more important as Ra is increased.

Indeed an important consequence of the convective motions is an increase of the heat flux ϕ crossing the layer. Below ΔT_c, ϕ is only due to the conduction $\phi = \phi_{cond}$. When the motion is present, the fluid velocity entails a supplementary heat flux ϕ_{conv}, and then the total heat flux $\phi = \phi_{cond} + \phi_{conv}$ is higher than it would be in a solely conductive state.

This is expressed by the Nusselt number:

$$Nu = \frac{\phi d}{\Lambda_T \Delta T} = \frac{\phi_{conv} + \phi_{cond}}{\phi_{cond}} \tag{17}$$

with Λ_T, the thermal conductivity of the fluid (see formula (1)).

So $Nu = 1$ provided that $Ra < Ra_c$; for $Ra \geqslant Ra_c$ the Nusselt number increases, reflecting the increasing part of the convection in the heat transport (Koschmieder and Pallas 1974, Ahlers 1974). An example is given in figure 21 (from Zamora and Rey de Luna 1984).

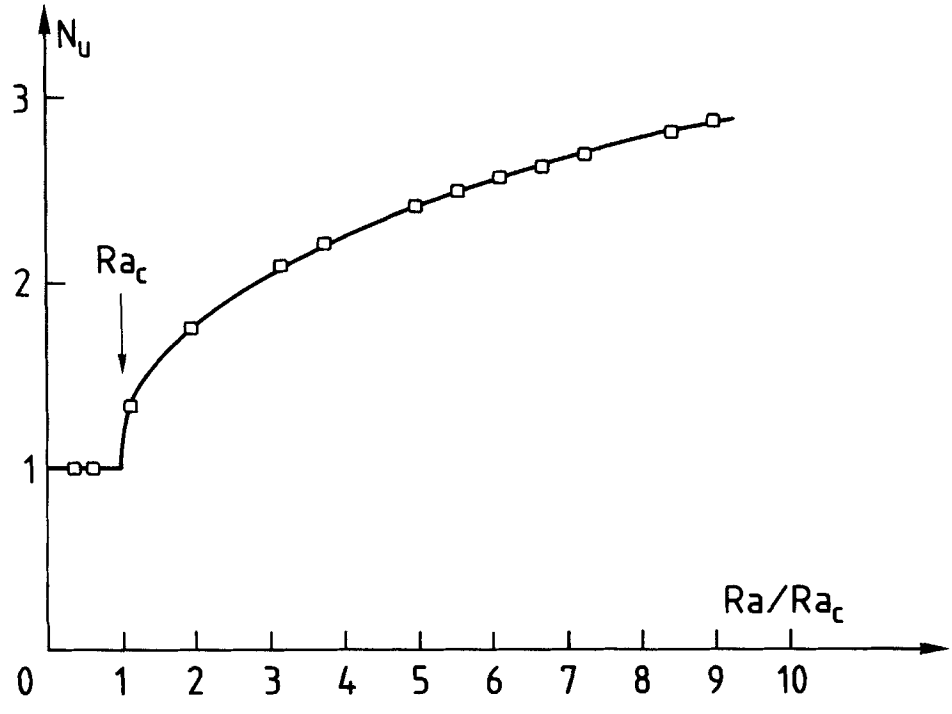

Figure 21. Variation of the Nusselt number versus Ra/Ra_c (Silicone oil $\nu = 3{\cdot}5$ stokes, from Zamora *et al.* 1984).

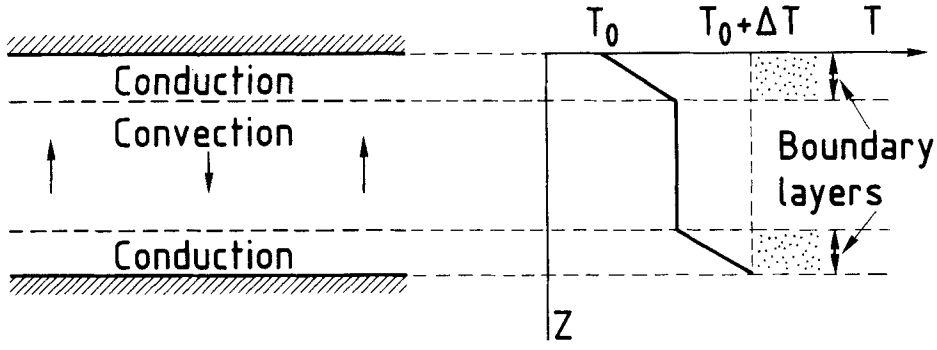

Figure 22. Schematic representation of the two thermal boundary layers.

Observation of what happens in the layer reveals that the process of heat transport depends on the position in the layer. In the central part ($z \sim d/2$), the vertical velocity V_z is large and the convection of the heat is dominant. By contrast, near the horizontal boundaries where V_z vanishes, the heat flux must be transported mainly by conduction; then it is natural that most of the thermal gradient will be concentrated in these two sublayers in order to favour conduction (see figure 22). These two sublayers, where the major part of the thermal gradient is applied, are called thermal boundary layers and play a leading role in subsequent instabilities occurring at high *Ra* numbers (at least with high *Pr* fluids).

4. Rayleigh–Bénard convection as a phase transition

4.1. *Stability diagram*

Up to now, we have seen that there is a transition at ΔT_c which consists in the establishment of convective motions. Moreover perfect structures (as well as imperfect ones, but locally for them) reveal the presence of a given spatial mode, under fixed conditions. This mode, defined by its wavenumber a or its wavelength Λ, is not unique. It depends not only on the Rayleigh number, but also on the Prandtl number of the fluid considered and on other parameters. So the problem is to know what are the stable modes of the system and how the preferred mode is chosen.

From a theoretical point of view, a good test is to investigate the response of the layer to an infinitesimal velocity disturbance δA such as a single Fourier mode (figure 23 (*a*))

$$\delta A = A \cos \frac{2\pi x}{\Lambda} \tag{18}$$

where x is an horizontal co-ordinate and Λ the wavelength of the Fourier mode which serves to test the stability of the layer. The problem now has two parameters, the Rayleigh number *Ra* and Λ the wavelength of the disturbance. The system is unstable if A increases with time for one or more values of Λ.

One usually assumes that:

$$A = A_0 \exp(\sigma t) \quad \text{with} \quad \sigma = f(\Lambda) \tag{19}$$

then $\sigma > 0$ means that an infinitesimal disturbance of given Λ is amplified so that the system is unstable.

$\sigma = 0$ means that the system is marginally stable (neutral stability)

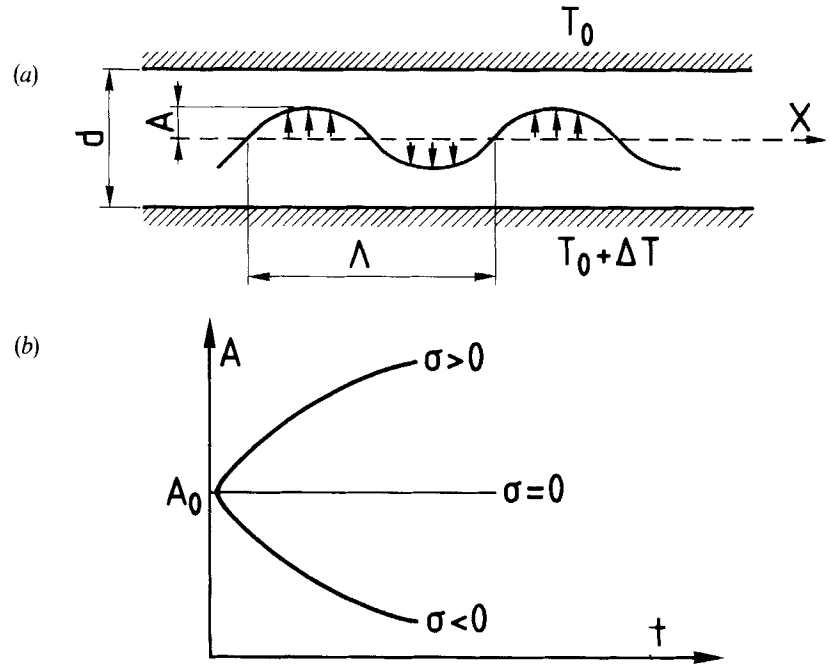

Figure 23. (*a*) Velocity perturbation with wavelength Λ, used to test the stability of the layer. (*b*) Time evolution of the amplitude of this perturbation for different σ.

$\sigma<0$ means that the system is stable, the initial disturbance of wavelength Λ being damped as shown schematically in figure 23 b.

The method of this linear analysis of stability is quite classical: the result is very important and shown schematically in figure 24 on a (Ra, a) diagram, a being the dimensionless wavevector of the Fourier mode $a=2\pi d/\Lambda$. In this figure, the curve of neutral stability is given by $\sigma=0$. All the points located below this curve correspond to a stable situation (no convection). The minimum Ra_c, a_c gives the critical onset of convection (for large containers), $Ra_c=1707$, $a_c=3{\cdot}117$.

This means that, near the critical onset Ra_c, the preferred mode for the convective structure is a Fourier mode of wavelength $\Lambda_c=2\pi d/a_c\simeq 2d$. But, in principle, for supercritical Ra numbers, a whole range of values of Λ is possible. In fact, a non linear analysis of the stability problem gives a curve which is inside the neutral stability curve (Eckhaus instability curve) so that the range of allowed Λ is restricted (in infinite geometry). The presence of lateral boundaries in the layer (the case of finite geometry of practical interest) restricts again the allowed range of Λ, though many questions remain today about this problem.

Nevertheless, the fact that only a small range of values of Λ is stable may be roughly understood by considering a criterion for optimization of the dissipation: too large a wavelength would increase the viscous dissipation on the horizontal part of the trajectories, while on the other hand too small a wavelength would increase by too much the horizontal heat flux between warm and cold streams. Outside the domain of stability for rolls, but inside the marginal stability curve, different instabilities may appear; these are defined by particular organizations of the motion (zig-zag, cross-rolls and others...) which generally tend to transform the actual wavenumber to a more

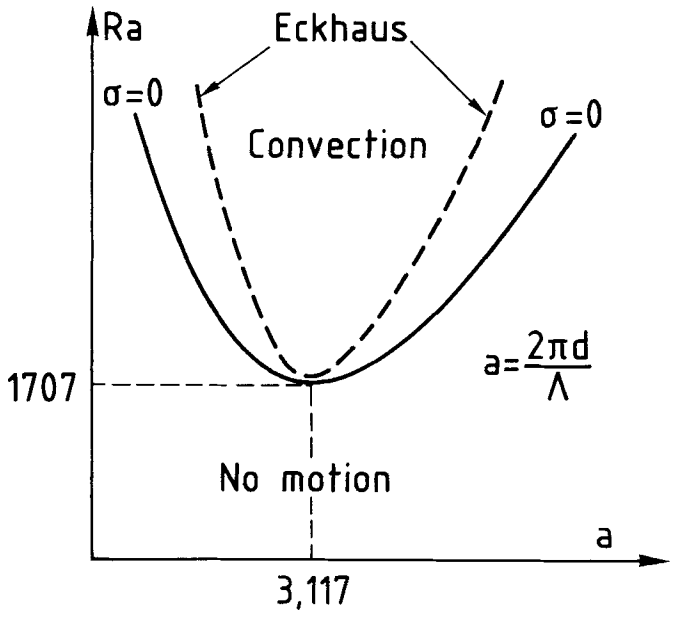

Figure 24. Stability diagram in the plane *Ra, a*. Full line represents the marginal stability curve, the dotted line the Eckhaus stability curve.

stable wavenumber (inside the stable domain of the rolls). The domain of existence of these different patterns varies with the Prandtl number; details can be found in the paper by F. H. Busse (1978).

4.2. *Mean field approach*

At Ra_c we have symmetry breaking between a disordered phase (null velocity, invariance of the properties of the layer to translations, high symmetry phase) and an ordered one (ordered rolls are present, the symmetry is lowered). This resembles, for example, a transition between the ferromagnetic and paramagnetic phases at the Curie point T_c, where in the ferromagnetic phase (of lower symmetry) the magnetization (order parameter) vanishes at T_c when the paramagnetic (higher symmetry) phase appears (figure 25). By analogy with the Landau approach to phase transitions, we can take the velocity V as the order parameter and define a Landau pseudo-potential which reflects the state of the system. We have seen that the stability of a physical system can be tested from its response to a small perturbation. A fluid layer is stable if a small velocity perturbation applied to the fluid relaxes to zero, as a ball placed on a concave surface returns to its equilibrium position at the bottom of this surface. Then the potential ϕ plotted versus the velocity V (see figure 26) should have its concavity upward in order to represent a stable state.

Following Landau, one expands ϕ as

$$\phi = \phi_0 + a_1 V + \frac{a_2}{2} V^2 + \frac{a_3}{3} V^3 + \frac{a_4}{4} V^4 + \ldots \tag{20}$$

We have previously seen that, in the Boussinesq approximation, upgoing streams have the same properties as downgoing streams. The invariance of the properties under

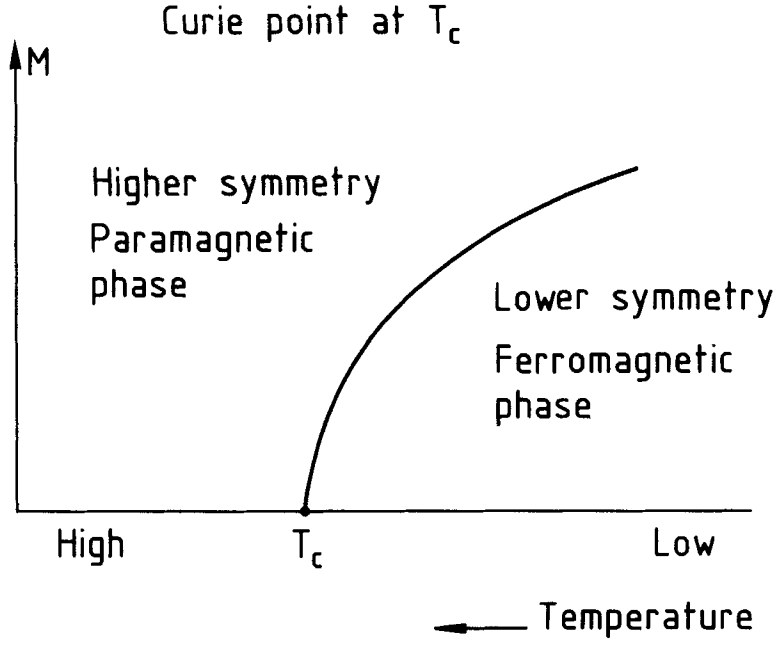

Figure 25. Magnetization M of a ferromagnet in the vicinity of the Curie point. This behaviour must be compared to that of the velocity amplitude as a function of Ra near the onset of the convection, see figure 28.

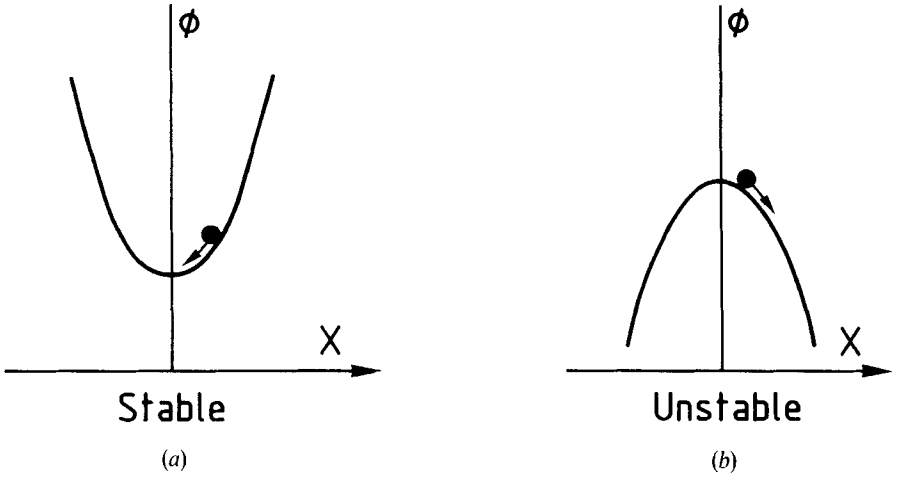

Figure 26. Scheme of the stability of a system according to the shape of the potential ϕ.

a change of V to $-V$ implies that ϕ must be invariant under the same change. So the odd terms must cancel and

$$\phi = \phi_0 + \frac{a_2 V^2}{2} + \frac{a_4 V^4}{4} \tag{21}$$

Since, when $Ra < Ra_c$, $V = 0$ then $a_2 > 0$ and for $Ra > Ra_c$, $V \neq 0$ and $a_2 < 0$, with a_2 varying as $(Ra - Ra_c)$; see figure 27.

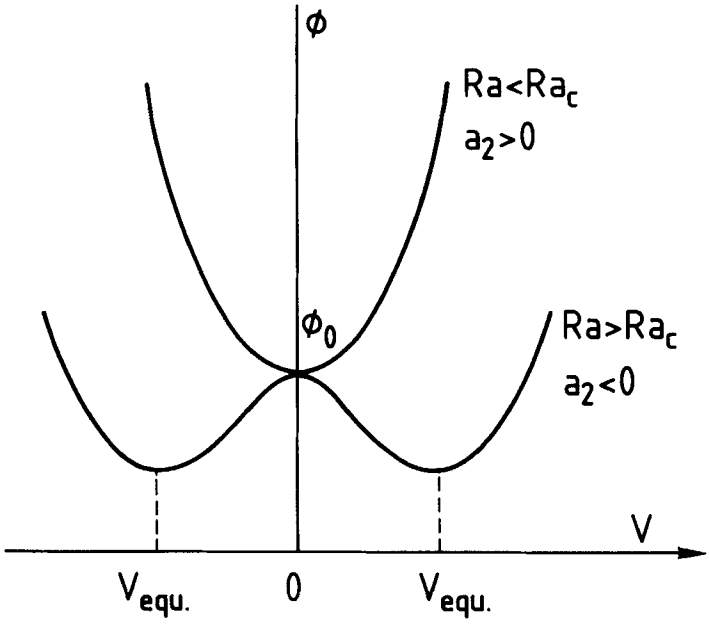

Figure 27. Dependence of the pseudo-potential Φ as a function of the velocity V for $Ra > Ra_c$ and $Ra < Ra_c$.

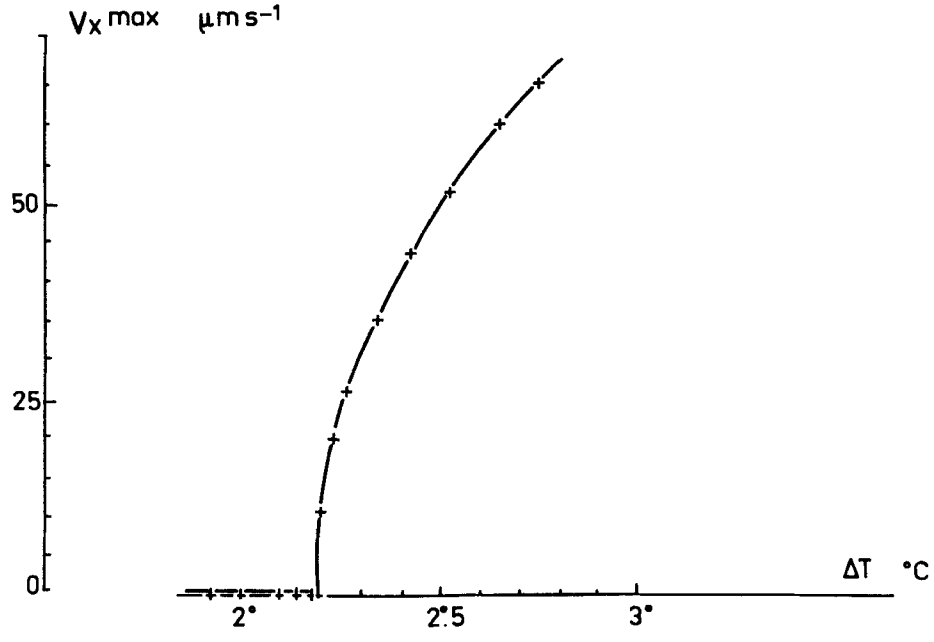

Figure 28. Variation of the maximum amplitude of the horizontal component of the velocity versus the temperature difference applied to the layer ($d = 1$ cm, silicone oil $\nu = 1$ stokes).

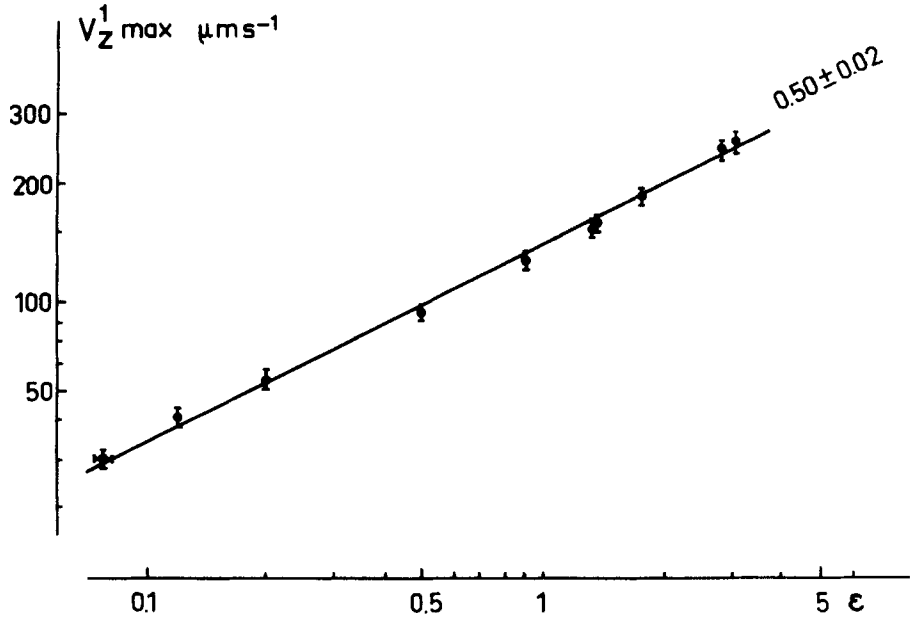

Figure 29. ε-dependence of the maximum vertical velocity component. ($d=1$ cm, $\nu \simeq 1$ stokes).

Steady equilibrium of the system is obtained for $d\phi/dV=0$. For $Ra > Ra_c$, we obtain three solutions for the velocity:

$V=0$ which is clearly unstable and

$$V=\pm\left(\frac{1}{a_4}\right)^{1/2}\left(\frac{Ra-Ra_c}{Ra_c}\right)^{1/2}=\pm\left(\frac{1}{a_4}\right)^{1/2}\varepsilon^{1/2} \tag{22}$$

with

$$\frac{Ra-Ra_c}{Ra_c}=\varepsilon.$$

This very important result shows that the equilibrium amplitude of the convective velocity has to vary as the square root of the departure from the threshold Ra_c. We find here the classical exponent $\beta=1/2$ of the convergence of the order parameter in a second order phase transition in the mean field approach. The measurements of the maximum amplitude of V_x and V_z are in very good agreement with this approach (Bergé 1976); in figure 28, we see clearly the existence of the threshold which corresponds here to $Ra_c=1600\pm100$. The variation of the velocity amplitude around the transition corresponds to a normal bifurcation (vertical tangent at the critical point ΔT_c) and the ε-dependence obeys very well the expected power law $\varepsilon^{1/2}$ (figure 29).

The exact value of the velocity amplitude, in the steady state, can be calculated from non linear theory. For the maximum value of the vertical V_z component (the maximum which is located at the mid-height of the layer $z=d/2$), it is found that far away from the influence of the lateral boundaries (Normand *et al.* 1977)

$$V_z=\frac{D_T}{d}\sqrt{2a^2}\left(\frac{Ra_c}{R^{(2)}}\right)^{1/2}\cos\frac{2\Pi x}{\Lambda}\cdot\varepsilon^{1/2}=V_z^1\cos\frac{2\Pi x}{\Lambda} \tag{23}$$

Here a is the wavenumber and $R^{(2)}$ is a polynomial function of the Prandtl number which, for $Pr \gg 1$ and $a = a_c$, is equal to $R^{(2)} = 2031$. Note that the velocity scales as $V \sim D_T/d$.

For $a = a_c = 3{\cdot}117$, $d = 1$ cm and a silicone oil with $D_T = 1{\cdot}14\ 10^{-3}\,\mathrm{cm^2\,s^{-1}}$ the calculated amplitude of the fundamental sinusoidal mode of convection is $V_z^1 = {}^{\circ}V_z\ (Z = d/2)$:

$$V_z^1 = 135\,\mu\mathrm{m\,s^{-1}} \quad \text{at} \quad \varepsilon = 1$$

For $a_c = 3{\cdot}117$ the cross-section of the rolls is a square and the maximum amplitude ${}^{\circ}V_x(z)$ at $z = 0{\cdot}22d$ and $z = 0{\cdot}78d$ (see figure 16 (*b*)), has within 2% the same value as V_z^1:

$$V_x^1 = 133\,\mu\mathrm{m\,s^{-1}} \quad \text{at} \quad \varepsilon = 1$$

The comparison between these theoretical results and the experimental measurements is excellent; for $d = 1$ cm and silicone oil, it was found for $\varepsilon = 1$ with $Pr = 900$:

$$V_z^1 \text{ measured} = 140 \pm 10\,\mu\mathrm{m\,s^{-1}}$$

$$V_x^1 \text{ measured} = 132 \pm 10\,\mu\mathrm{m\,s^{-1}}$$

The amplitudes of the second and third harmonics modes $V2$ and $V3$ respectively have also been calculated (Busse 1967 a, Dubois *et al.* 1978 b); it is expected that $V2$ should vary as ε and $V3$ as $\varepsilon^{1{\cdot}5}$. The measurements of these amplitudes by spatial Fourier analysis have given results in good agreement with these predictions (see figure 30) (Dubois and Bergé 1978). These amplitudes depend on the actual wavenumber and the experimental results agree with the Busse calculations.

Let us return to the Landau potential in order to look now at the transient behaviour of the velocity.

If we set: $a_4 = 1/V_0^2$

We get:

$$\phi = \phi_0 - \varepsilon \frac{V^2}{2} + \frac{1}{V_0^2} \frac{V^4}{4}. \tag{24}$$

The dynamical response can be found if we notice, by analogy with what happens to a ball displaced from its equilibrium position at the bottom of a concave surface, that

$$\frac{\mathrm{d}V}{\mathrm{d}t} = -\Gamma \frac{\mathrm{d}\phi}{\mathrm{d}V} \tag{25}$$

For dimensional reasons ($[\phi] = L^2T^{-2}$) Γ is the reciprocal of a characteristic time $\Gamma = \tau_0^{-1}$ and finally one gets

$$\tau_0 \frac{\mathrm{d}V}{\mathrm{d}t} = \varepsilon V - \frac{V^3}{V_0^2}. \tag{26}$$

From this equation we can derive the transient behaviour of V: at small ε value and short times (V small, $V^3 \ll V$), $\tau_0\,\mathrm{d}V/\mathrm{d}t \simeq \varepsilon V$ meaning that the initial slope $\mathrm{d}V/\mathrm{d}t$ tends to zero with ε; then the response time of the instability diverges at $\varepsilon = 0$ as:

$$\tau = \tau_0 \varepsilon^{-1} \tag{27}$$

This fundamental phenomenon is named 'critical slowing down' by analogy with what happens in critical phenomena where the time dependence of the spontaneous

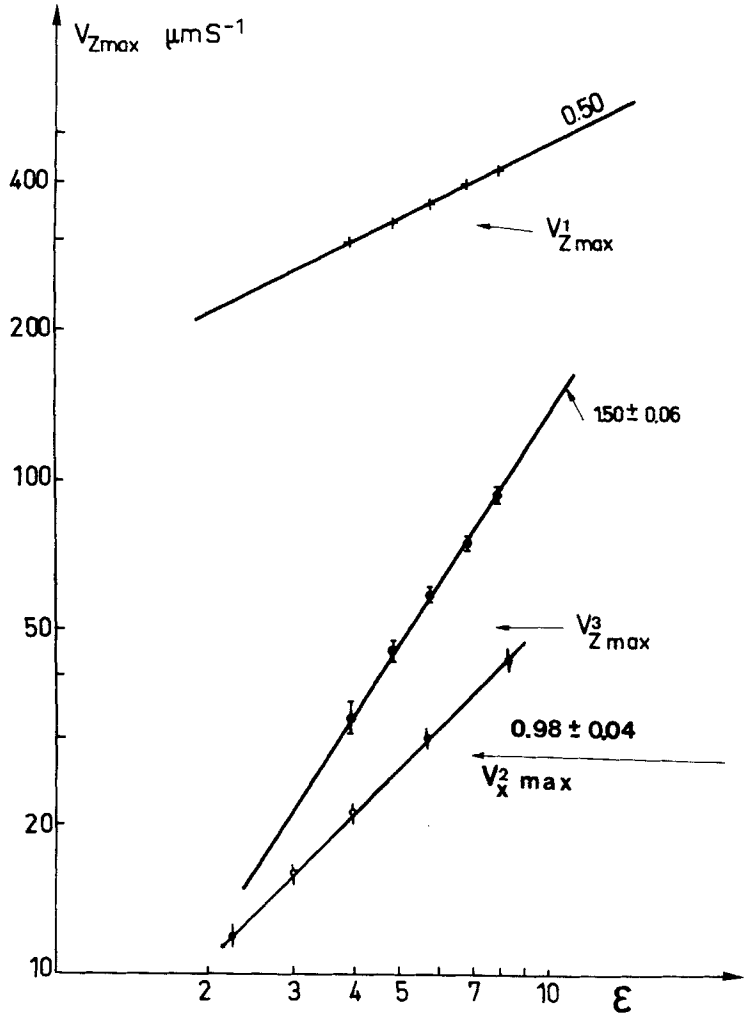

Figure 30. ε-dependences of the amplitude of the harmonic modes in comparison with that of the fundamental mode ($d = 1$ cm, $\nu \simeq 1$ stokes $a = a_c$).

fluctuations is considerably slowed near the critical point. Notice that for long times, the amplitude V tends to a limit owing to the non-linear terms in the amplitude equation.

τ_0 scales as d^2/D_T, the vertical thermal diffusion time of the layer, and its value is:

$$\tau_0 = \frac{d^2}{D_T} \frac{1 + 1{\cdot}954\,Pr}{38{\cdot}44\,Pr} \quad \text{(rigid-rigid boundaries).} \tag{28}$$

In the case of Rayleigh–Bénard convection, that means that if we perturb the fluid by rapidly increasing the temperature difference ΔT by a small amount, the subsequent evolution to the new equilibrium will show an exponential time dependence with a characteristic time τ which depends on the ε value (Sawada 1978, Wesfreid *et al.* 1978). Measurements at different Rayleigh numbers have given the variation shown in figure 31 in the case of experiments with silicone oil. The power law $\tau = \tau_0 \varepsilon^{-1}$ is accurately

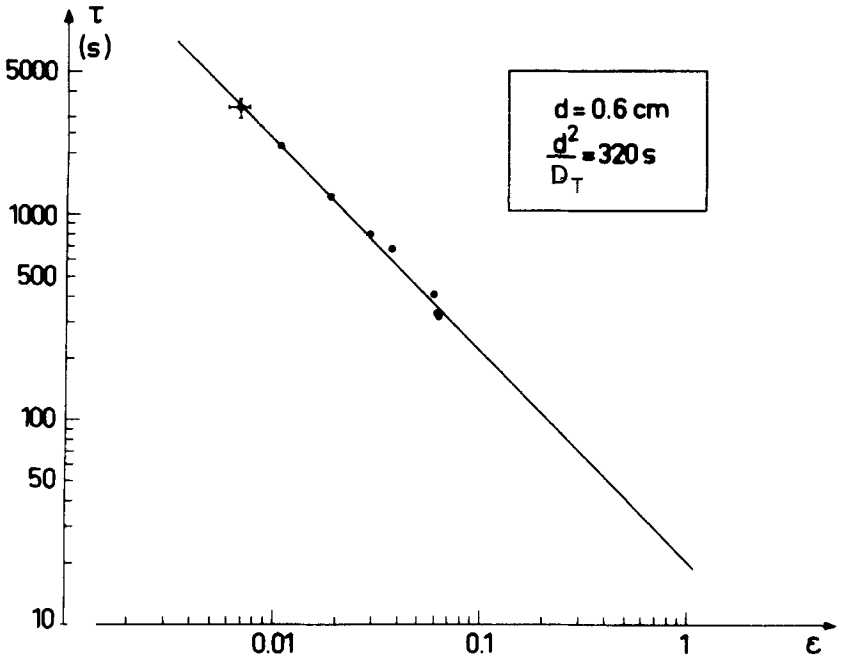

Figure 31. ε-dependence of the convective characteristic time.

verified and the value of τ_0 is in good agreement with the expected value. (In the case reported here, τ_0 calculated from the experiment is $\tau_0 = 20 \pm 4$ sec), (Wesfreid *et al.* 1978).

4.3. *More about the critical properties: the spatial effects*

In addition to the critical slowing down, second order phase transitions are characterized by critical spatial correlation effects: more precisely, if the order parameter is locally perturbed from its mean value, this perturbation occupies in fact some spatial extension in the critical medium; this extension is measured by the correlation range ξ which diverges when the critical point is approached. In the Rayleigh–Bénard instabillity the analogy is the following: far from the lateral boundaries we have a sinusoidal Fourier component with an asymptotic amplitude V^1. In contrast, near a lateral boundary the amplitude of this Fourier mode has to vanish ($V=0$ at all the boundaries). The question is: what is the spatial extent of the perturbation ($V=0$) imposed by the lateral boundaries? The answer can be found in the marginal stability curve $Ra=f(a)$. At a given supercritical Ra number, we have a finite range Δa of allowed wavevectors. The fit with $V=0$ at $x=0$ (boundary) and $V=V^1$ far from the boundary is simply related through a Fourier transform between the reciprocal space (a) and the direct space (x) (see figure 32).

A range Δa of wavevectors implies a spatial width for the modulation of the sinusoide $V=f(x)$ which is

$$\xi \sim \frac{1}{\Delta a} \tag{29}$$

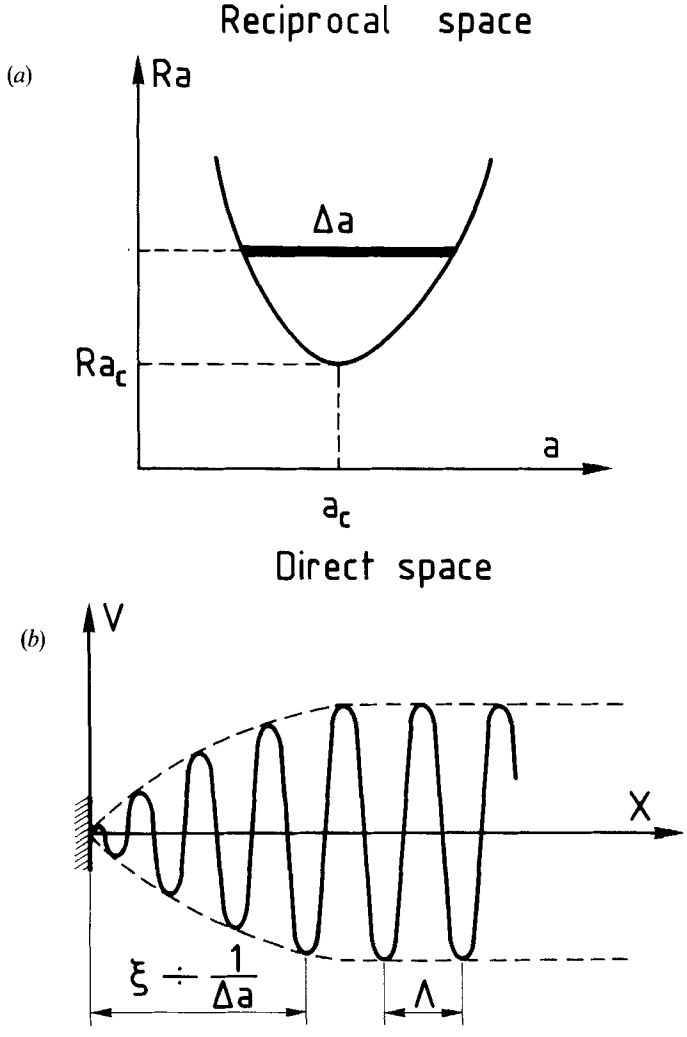

Figure 32. Spatial correlation effect. The correlation length ξ in the direct space is inversely proportional to the allowed bandwidth Δa inside the marginal stability curve.

Approximating the $Ra=f(a)$ marginal stability curve by a parabola means that

$$\Delta a \simeq (Ra - Ra_c)^{1/2}, \tag{30}$$

then

$$\xi \sim \xi_0 (Ra - Ra_c)^{-1/2}. \tag{31}$$

The supercritical correlation length ξ^+ diverges when $Ra \to Ra_c$ with a classical exponent ν in the field of critical phenomena ($\nu = 1/2$ in the mean field approach).

Thus, the perturbation of a lateral boundary affects the amplitude of the envelope of the spatial dependence $V=f(x)$ up to distances of about ξ^+ which can be large if we are near the threshold Ra_c. Then a negative curvature of the envelope, $\partial^2 V/\partial x^2 < 0$, is produced.

In the same manner, if, instead of perturbing rolls by imposing $V=0$, we perturb a quiescent layer which is slightly subcritical ($Ra < Ra_c$) by a local velocity, we can induce spatially damped rolls (subcritical rolls) over a range of about ξ^-, ξ^- having the same critical dependence as ξ^+, the supercritical correlation length. Here, by inducing subcritical damped rolls, we impose a positive curvature on the envelope i.e. $\partial^2 V/\partial^2 x > 0$.

So, in order to account for the spatial effects, we have to add a term in the amplitude equation such as

$$\tau_0 \frac{dV}{dt} = \varepsilon V - \frac{V^3}{V_0^2} + \xi_0^2 \frac{\partial^2 V}{\partial x^2} \tag{32}$$

for $\varepsilon > 0$ and ε should be replaced by $-|\varepsilon|$ for $\varepsilon < 0$.

This term $\partial^2 V/\partial x^2$ due to spatial inhomogeneities acts as a force term. When it is negative, it represents a stabilizing effect; when it is positive it may balance the stabilizing effects (dominant when $\varepsilon < 0$) and induce motions.

Exact solutions of this equation show that the envelopes are the following:

$$\text{for} \quad \varepsilon > 0 \quad \text{and} \quad V = 0 \quad \text{at} \quad x = 0$$

$$V = V^1 \tanh \frac{x}{\xi^+} \tag{33}$$

with

$$\xi^+ = \sqrt{2}\xi_0 \varepsilon^{-1/2};$$

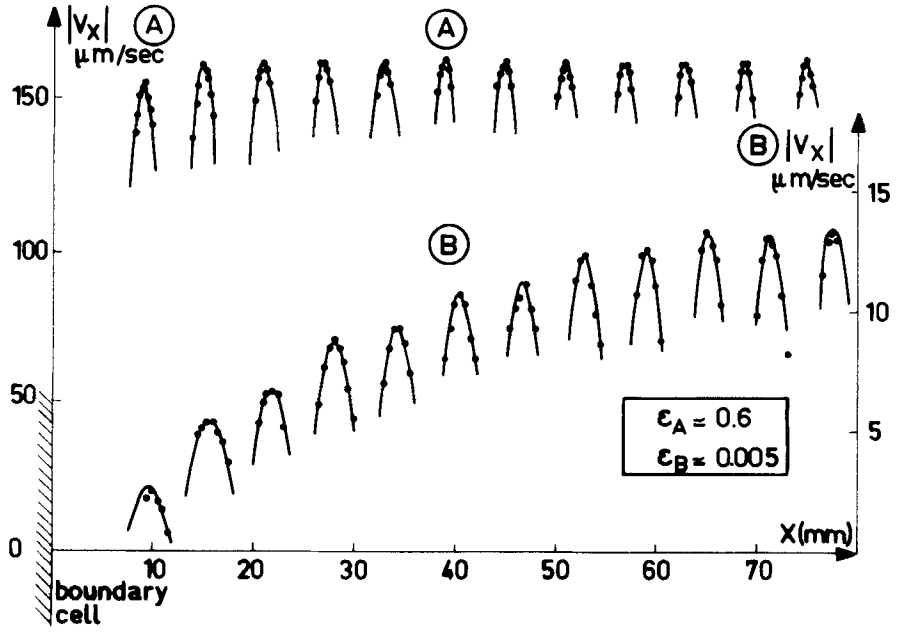

Figure 33. Velocity amplitude versus the distance x to the lateral boundary, for two ε values (Si oil $\nu = 0{\cdot}56$ stokes). Note the strong influence of the boundary for the lower ε value which extends for 10 rolls.

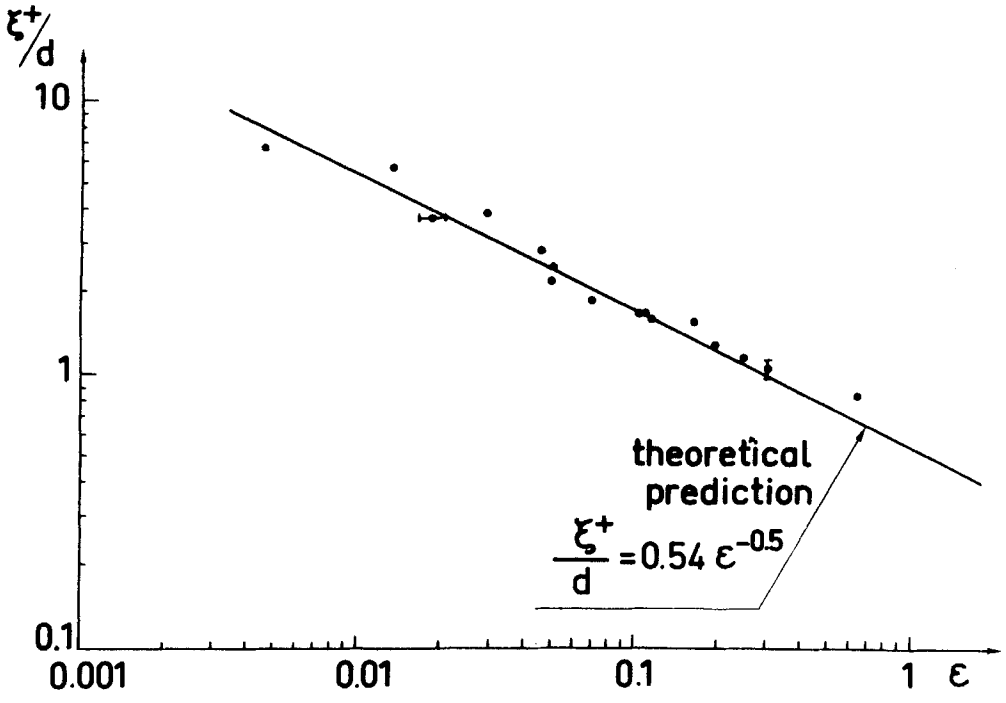

Figure 34. Log-log plot of the measured correlation length versus ε for supercritical Ra values.

for $\varepsilon<0$ (subcritical induced rolls) and $V=V_B$ at $x=0$

$$V=V_B\exp(-|x|/\xi^-) \tag{34}$$

with

$$\xi^-=\xi_0|\varepsilon|^{-1/2}.$$

ξ_0 is an universal value, for as we have said before, it is only related to the marginal stability curve; $\xi_0=0{\cdot}385d$.

Measurements have shown these spatial dependences and their properties (Wesfreid *et al.*, 1978). In figure 33, one can see the spatial dependence of V_x on distance to a boundary of the cell for two values of ε. For the higher value of ε ($\varepsilon=0{\cdot}6$), the behaviour of the velocity is essentially represented along the whole cell by sinusoidal dependence $V=V^1\sin(2\pi x/\Lambda)$ as previously reported. In contrast, for the lower value of ε ($\varepsilon=0{\cdot}005$) the boundary effect penetrates deeply into the cell affecting about 10 rolls.

The envelopes of the measured $V=f(x)$ dependences are in very good agreement with the expected law $V_x\sim\tanh(x/\xi^+)$, from which ξ^+ can be calculated for different ε values. A log log plot of ξ^+ versus ε (figure 34) shows not only that the power law is well obeyed in the experimental situation but also that the value of ξ_0 is exactly that obtained by the calculation.

Experiments on induced pretransitional rolls ($Ra<Ra_c$) have been performed by imposing a local vertical velocity on an otherwise quiescent subcritical layer (Wesfreid *et al.* 1979), as can be seen in figure 35, where damped rolls are induced by a vertical stream in the centre of the layer. The envelopes of the velocity dependences are exponential as $\exp[-|x-x_0|/\xi]$ with x_0 the abscissa of the inducing stream. The value

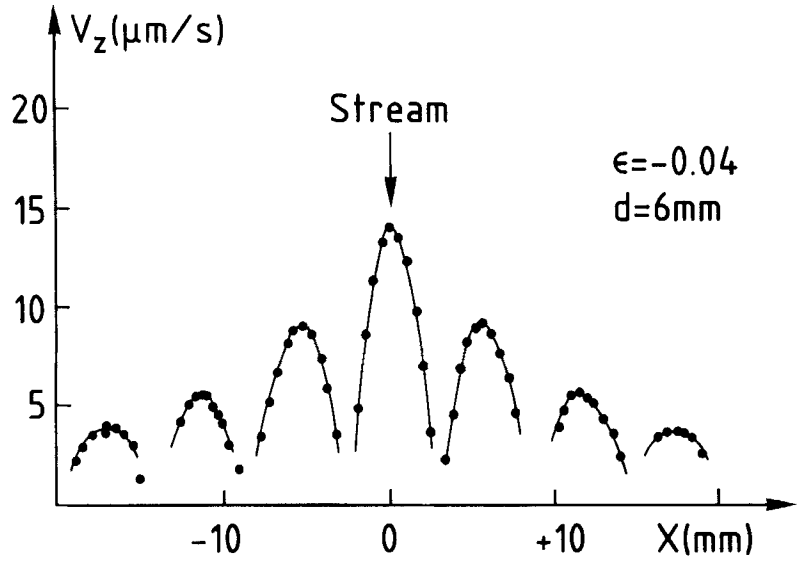

Figure 35. Velocity profile of induced rolls for $Ra < Ra_c$. The induction has been made by a thin jet crossing vertically the layer as indicated by the arrow on the figure.

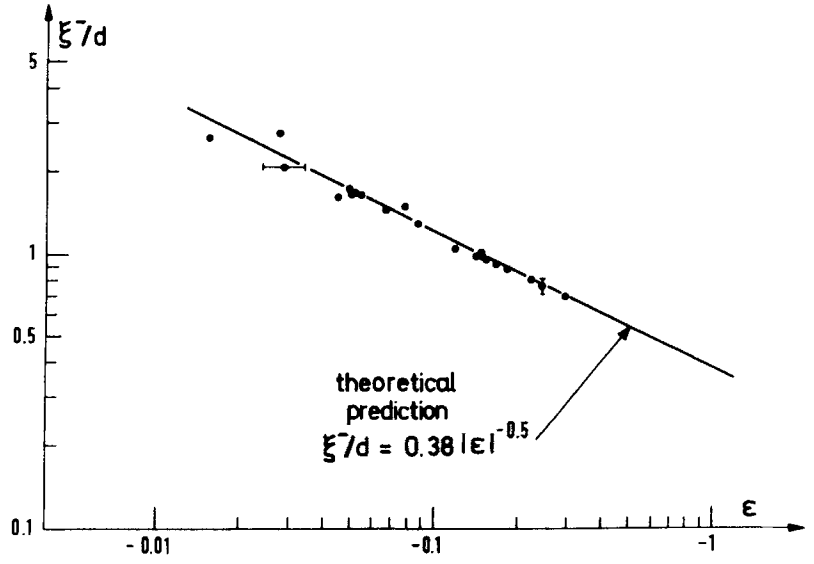

Figure 36. Log-log plot of the measured correlation length versus ε for subcritical *Ra* values.

of ξ^- deduced from these profiles at different ε values shows good agreement with the theoretical prediction (see figure 36).

To summarize the convective properties near the threshold we have to return to the fundamental amplitude equation (32)

$$\tau_0 \frac{dV}{dt} = \varepsilon V - \frac{V^3}{V_0^2} + \xi_0^2 \frac{\partial^2 V}{\partial x^2}$$

valid in the simplest case of stable and perfect two-dimensional rolls.

Then, in these conditions, the Rayleigh–Bénard convection can be entirely described with three parameters, at least near threshold:

(*a*) The order parameter i.e. the velocity amplitude which grows as $\varepsilon^{1/2}$.
(*b*) The time response τ to a perturbation, which exhibits a critical slowing down such as $\tau=\tau_0\varepsilon^{-1}$.
(*c*) The influence length which controls the spatial response to a local perturbation and which diverges as $\xi_0\varepsilon^{-1/2}$.

4.4. *Non-Boussinesq convection*

If the physical properties of the convective fluid depend strongly on the temperature, i.e. they are different at the top and at the bottom boundaries, there is an asymmetry between the upward and the downward motions as we have already seen. Then the Landau potential ϕ has to keep the odd terms in the expansion

$$\phi=\phi_0+a_1V+\frac{a_2}{2}V^2+\frac{a_3}{3}V^3+\frac{a_4}{4}V^4 \tag{35}$$

from which we obtain an amplitude equation for the velocity V

$$\tau\frac{dV}{dt}=\varepsilon V-a_3V^2-a_4V^3 \tag{36}$$

with $a_4>0$.

We are in the presence of a subcritical bifurcation (see figure 37). In the stationary state the solution for the velocity amplitude is

$$V=\frac{V_0}{2}\pm\frac{V_0}{2}\left[1+2\frac{V_1}{V_0}\varepsilon+\ldots\right] \tag{37}$$

where V_0 is the nonzero value at $\varepsilon=0$ ($V_0=a_3/a_4$) and V_1 the value at $\varepsilon=1$. In fact, we have only to consider the solution $V=V_0/2+V_0/2[1+\ldots]$ which is the only stable one. This value is that of the amplitude of the velocity at the centre of the hexagons which form the pattern; the amplitude of the velocity of opposite sign, in the periphery of the hexagons, is smaller as shown in figure 7 and figure 38 (conservation of the flux).

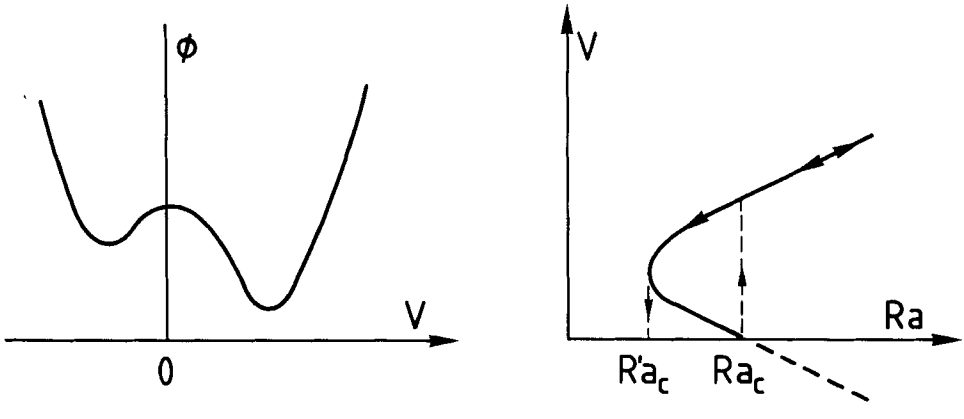

Figure 37. Non-Boussinesq convection. On the left: the corresponding asymmetric pseudo-potential. On the right: the scheme of the related subcritical bifurcation.

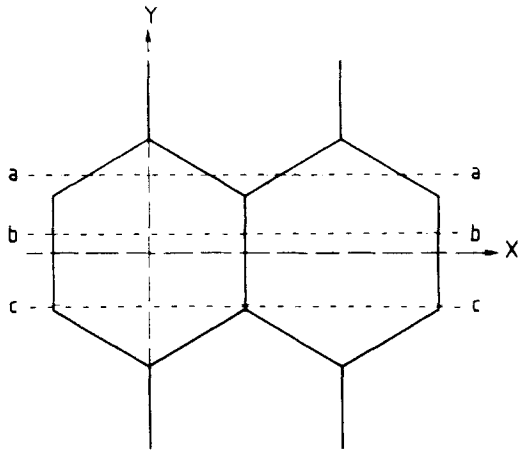

(*a*)

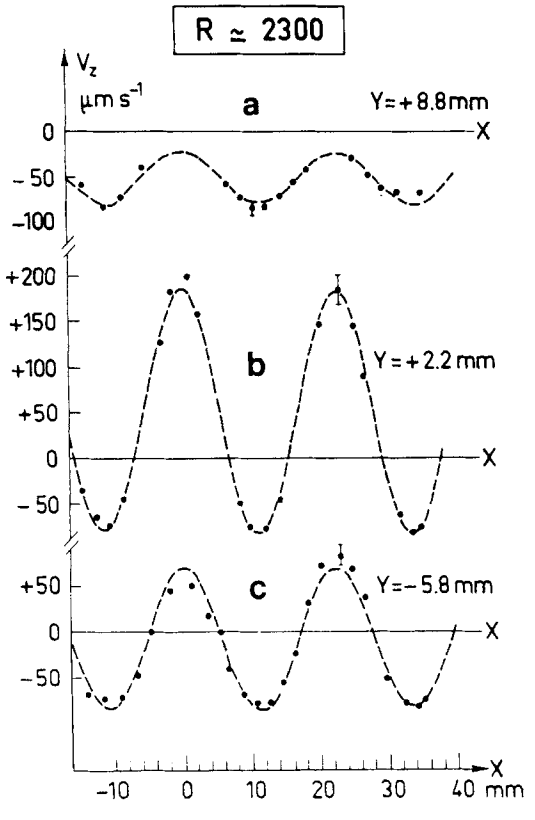

(*b*)

Figure 38. Velocity profiles in a hexagonal pattern. Measurements have been performed at the mid-height plane along three lines as indicated on (A). (Water, temperature at the top plate: 4°C, $d = 1$ cm).

The behaviour is then like that of a transition of first order: at a given value Ra_c (which may be different from 1707), there is a jump from $V \equiv 0$ to $V = V_0$. Then, for low value of ε, there is a linear variation of V with ε. When Ra is decreased, there is hysteresis, and the motion disappears at a value $Ra'_c < Ra_c$, corresponding to a negative value $\varepsilon' = -V_0/4V_1$. This behaviour with hexagonal pattern was observed for various liquids (Somerscales and Dougherty 1970), (Hoard *et al.* 1970), and also with water near 4°C for which the volume expansion coefficient was null at the top plate (M. Dubois *et al.* 1978 c). Meanwhile, the hexagonal pattern is only stable in a small ε domain: when Ra is increased, there is further transformation of the hexagons into rolls, as predicted in the paper by F. H. Busse (1967 b). The principal reason for this transformation lies in the fact that hexagons are less efficient for heat transport than are the rolls.

5. Dynamics of spatial organization

Up to now, the basic properties of the convective state have been discussed in the framework of perfect structures near threshold, i.e. parallel two-dimensional rolls, whose variables at the equilibrium state are only a function of x and z. We now consider the properties of natural structures, with defects, for which the whole pattern in the x, y plane has to be taken into account; then the formulation becomes three-dimensional and the calculations more complicated (Cross 1982)†. Note that if the profile along z is not considered, patterns in the x, y plane are two dimensional and comparisons may be imagined with two dimensional crystals. This concept; in particular, is dominant in some numerical studies (Manneville 1983).

The two main problems with natural structures relate to the formation of the pattern and its dynamics. It was observed that, just after the convection has set in, there is a slow relaxation of the structure, which involves the motion of defects and the rearrangement of the pattern; this process takes a time which may be very long and is often very much longer than the horizontal diffusion time, this being of order L^2/D_T for a container of size L. Nevertheless in the limit of the observations to date with moderate and high Prandtl number fluids, it seems that the structure reaches a stationary equilibrium state, with the presence of some remaining defects (see for example figure 11). On the other hand, with low Prandtl numbers fluids (helium (Ahlers and Behringer 1978), mercury (Fauve *et al.* 1984)), it was observed that the chaotic state persists, giving a convective turbulent motion near threshold. Very few experimental data about this kind of turbulence are presently available.

Thus, many questions remain unanswered about disordered structures, even at threshold. A first step has recently been made by the study of the dynamical behaviour of isolated defects in otherwise quasi-perfect structures and with high Pr fluids.

5.1. *Diffusive modes in Rayleigh–Bénard structures*

We look first at the stability of the regular periodic pattern against phase modulations. When the convective motions are spatially organized in a well ordered structure, the local velocity amplitude may be described by a single horizontal mode with

† The presence of vertical vorticity, introduced by the three-dimensional aspect of the structure, generates secondary flows on the large scale—large compared to d— which have to be taken into account. Their influence will be higher as the Prandtl number is lower.

wavenumber a, at least far from the boundaries. So the vertical velocity component varies in a horizontal plane, along a direction **x** perpendicular to the roll axis as

$$V_z = {}^{\circ}V_z \cos[ax + \varphi(x, y, t)] \tag{38}$$

${}^{\circ}V_z$ being the Fourier amplitude of the velocity, and φ the phase defining the roll position.

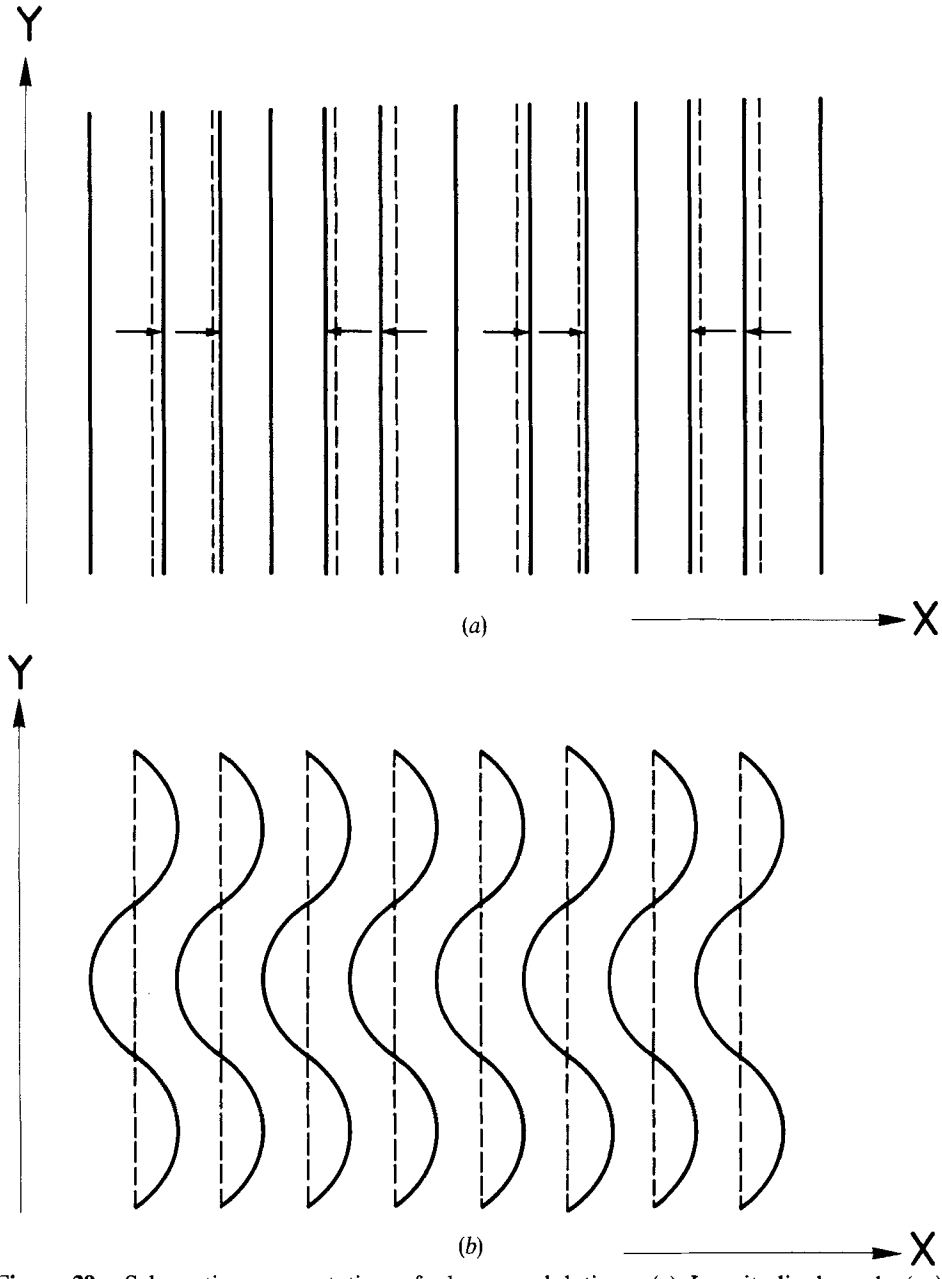

Figure 39. Schematic representation of phase modulations. (*a*) Longitudinal mode ($q_{\parallel}$). (*b*) Transverse mode ($q_{\perp}$). (The dotted lines represent the unperturbed pattern).

We can purposely perturb the phase φ of the roll pattern in order to study the dynamics of the phase φ of the periodic rolls, just as in the periodic arrangement of atoms in a crystal, we can study the dynamics of elastic waves. In the Rayleigh–Bénard 'crystal' we can perturb the rolls (i.e. modulate the phase φ) according to two modes: one with a wavevector $\mathbf{q}_{\parallel}$ along the x axis, the second with a wavevector $\mathbf{q}_{\perp}$ along the y axis (see figure 39).

One can see that the first $\mathbf{q}_{\parallel}$ mode corresponds to a periodic compression and expansion of the roll structure (like a sound wave); this $\mathbf{q}_{\parallel}$ mode is longitudinal. The second mode $\mathbf{q}_{\perp}$ corresponds to a deformation of the rolls with a 'zig-zag' shape: $\mathbf{q}_{\perp}$ corresponds to a transverse mode, these two modes can be described by phase modulations such as:

$$\text{— longitudinal mode: } \varphi = \varphi_0 \cos(q_{\parallel} x), \tag{39}$$

$$\text{— transverse mode: } \varphi' = \varphi'_0 \cos(q_{\perp} y). \tag{40}$$

The main difference from what happens in an ordinary crystal corresponds to the fact that in the Rayleigh-Bénard case (when the Prandtl number is large) the dynamics of phase perturbations is not propagative but diffusive: the system of rolls behaves as if the dissipation completely damps the motion, leading to a diffusion mechanism.

The equation of phase diffusion has been theoretically derived in the Rayleigh–Bénard case (Pomeau and Manneville, 1979) (Cross 1983)

$$\frac{\mathrm{d}\varphi}{\mathrm{d}t} = D_{\parallel} \frac{\partial^2 \varphi}{\partial x^2} + D_{\perp} \frac{\partial^2 \varphi}{\partial y^2} \tag{41}$$

where $D_{\parallel}$ and $D_{\perp}$ are the phase diffusion coefficients related to the longitudinal and the transverse modes respectively.

The dynamics of the relaxation (or amplification) of phase perturbations is then given by exponential variations of the form:

$$\varphi = \varphi_0 \exp -Dq^2 t \tag{42}$$

with characteristic times

$$\tau_{\parallel} = (D_{\parallel} q_{\parallel}^2)^{-1} \tag{43}$$

and

$$\tau_{\perp} = (D_{\perp} q^2)^{-1} \tag{44}$$

respectively.

We now must see how these predictions have been checked experimentally. In the experiment reported by V. Croquette and F. Schosseler (1982), the fluid (silicone oil) was confined in a rectangular plexiglass frame such that $L_x = 20d$, $L_y = 12d$, with d the depth of the layer, equal to 0·5 cm and corresponding nearly to the fact that a large aspect ratio cell must be taken to approximate as well as possible to the infinite geometry (which is the assumption of the theory).

In order to see the structure from above as well as to induce thermally the perturbed roll structure according to a well defined phase mode (as previously described) the top plate is of sapphire, transparent but a good thermal conductor, while the lower one is of polished copper (see figure 40). The whole structure was made visible from above by classical shadowgraphy and precise phase motions were detected by laser anemometry.

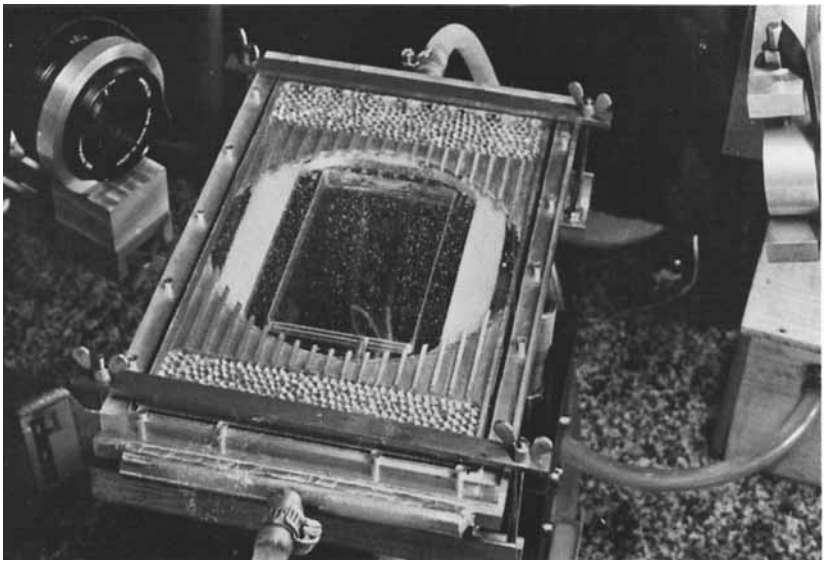

Figure 40. Photograph of a typical cell used for structure visualizations. The thermal regulation at the top (sapphire plate) and at the bottom (copper plate) is achieved by circulating water from thermostatic baths.

Structures with a longitudinal or a transverse phase modulation were induced and the evolution of this modulation was studied, whence the dynamics of both modes were determined.

5.1.1. *Longitudinal modes*: The evolution of the longitudinal phase modulation was studied for two $q_{\parallel}$ values ($2\pi/L_x$ and $4\pi/L_x$) with $a=a_c$. As expected, the phase relaxation was found to be exponential with a characteristic time τ_q which varies quadratically with $q_{\parallel}$; thus the dispersion relation (43) is confirmed. $D_{\parallel}$, calculated from the measurements of $\tau_{\parallel}$ was: $D_{\parallel}=1{\cdot}7\pm0{\cdot}5\,10^{-3}\,\mathrm{cm^2\,s^{-1}}$ in reasonably good agreement with the theoretical prediction, ($2{\cdot}23\ 10^{-3}\,\mathrm{cm^2\,s^{-1}}$), as given by the relation

$$D_{\parallel}=\frac{\xi_0^2}{\tau_0}\frac{(\varepsilon-4{\cdot}31\delta^2/a^2)}{(\varepsilon-1{\cdot}44\delta^2/a^2)} \tag{45}$$

with $\delta=a-a_c$. When $\delta/a\ll1$, $D_{\parallel}$ equals 2·92 times $D_{\perp}$.

The positive value of $D_{\parallel}$ reflects the high stability of the roll structure against compression or expansion deformations. The maximum of stability holds for the maximum value of $D_{\parallel}$ i.e. for $a=a_c$. Inside the curve of the Eckhaus instability $D_{\parallel}$ remains positive but on the curve it vanishes (see figure 24); then, outside this region, $D_{\parallel}$ becomes negative and a phase modulation would grow exponentially instead of decaying.

5.1.2. *Transverse modes*: It is far more difficult to perform quantitative measurements for the transverse mode, because of its critical dependence on $(a-a_c)$. Recent calculations (Manneville and Piquemal 1983) have given the following complete expression for $D_{\perp}$

$$D_{\perp}=\left(\frac{\xi_0^2}{\tau_0}\right)\left(\frac{\delta}{a_c}\right)+C\varepsilon \tag{46}$$

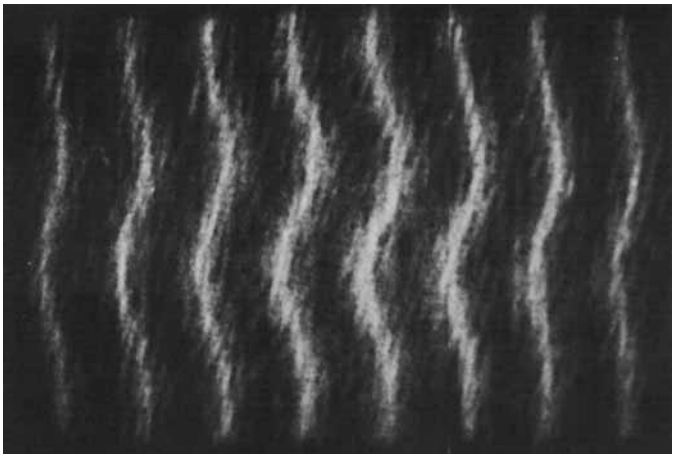

Figure 41. Induced structure with zig-zag modulation before phase relaxation. (Silicone oil $\nu = 0{\cdot}1$ stokes, $d = 5$ mm).

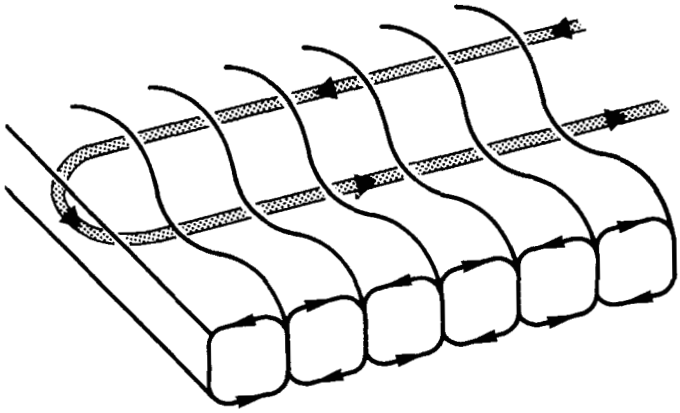

Figure 42. Schematic illustration of secondary flow (broad line) associated with the curvature of the rolls.

C is a quantity which depends on the Prandtl number and which may be taken as zero in the limit of infinite Prandtl number.

Moreover, in an experimental situation, the effect is complicated by boundary effects. The results we report here correspond to the evolution of a zig-zag structure taking into account the two basic boundary effects: the phase modulation must vanish in the vicinity of the sidewalls ($x = 0$ and $x = L_x$) and the roll axes must be perpendicular to the sidewalls at $y = 0$ and $y = L_y$. A photograph of the structure is shown schematically in figure 41 which corresponds to $q_\perp = 4\pi/L_y$.

In this experiment, the main aim was to point out the dependence of $D_\perp$ with a. The time evolution was once more an exponential relaxation except in the case of no evolution or amplification of the modulation.

Results are presented in table 2 ($(Ra - Ra_c)/Ra_c \simeq 0{\cdot}6$).

a/a_c	1·1	1	0·9	0·8
τ	500 s	1 600 s	∞	amplification

Table 2.

For $a/a_c = 0{\cdot}9$, τ becomes very large meaning that the induced modulation neither grows nor relaxes and for $a/a_c = 0{\cdot}8$ the modulation grows rather than relaxing. The phase modulation is then amplified, leading to the 'zig-zag' instability described by F. H. Busse (1978).

Despite the low value of $D_\perp$ (around ten times smaller than that of $D_\parallel$), the diffusion coefficient $D_\perp$ plays a very important role in the formation of the pattern. It intervenes in the force which acts on the curvature of the rolls axis and then in those which control the dynamics of defects, in particular dislocations, as we shall see later.

5.2. *Wavenumber selection*

The natural structures are not strictly periodic, though the size of the rolls is relatively homogeneous in the whole pattern; so it is not possible to associate with them a single wavevector. On the other hand they may be described by a wave packet, i.e. a distribution of wavevectors, which may be directly deduced from the two dimensional Fourier spectra of the structure, as described by Gollub and McCarriar (1982 b). In this situation, the wavenumber selection corresponds to the fact that this distribution is centred on a well defined wavevector a_s and that the width of the distribution is quite narrow compared with the extension of the stable roll domain defined by F. H. Busse (Busse and Whitehead 1971, Busse 1978).

Moreover, as already stated, the mean wavenumber a_s depends on the Rayleigh number so that it is possible to say that the structure actually 'chooses its wavenumber'.

Theoretically the problem of this selection is far from easy. The first attempt based on the idea that the structure selects the wavenumber which maximizes the heat flux transported by the convection leads to predictions in total contradiction with the experiments. Recently the problem has received more accurate treatments but confrontation with experimental results is still needed to test the new ideas.

Why is this problem so delicate in case of convection? If we compare convection with what happens in crystals the dependence of the size of the unit cell of a crystal on its temperature no longer has any secret for the physicists. Crystals possess a free-energy function whose minimum at a given temperature defines completely the state of the system, i.e. the dimension of its unit cell. This is not the case for convective patterns for which it is not possible to find such a function, the best proof being that these patterns might oscillate or become turbulent and such a state cannot be described as the minimum of any potential.

Several mechanisms have been proposed as responsible for the wavenumber selection. Some are related to the boundary conditions, such as the influence of the lateral boundaries which may extend to the whole pattern (Cross *et al.* 1983). In the same way, a slow spatial modulation of the Rayleigh number may favour the selection of a unique wavenumber (Cannel *et al.* 1983).

Intrinsic convective properties may also be responsible for the choice of the wavelength; two examples are given in the next paragraph. The choice of the preferred mode is revealed in such cases by the motion of defects.

5.2.1. *Motion of dislocations*: To study the motion of dislocations, the simplest manner is to look at the evolution of a quasi perfect structure containing only one dislocation.

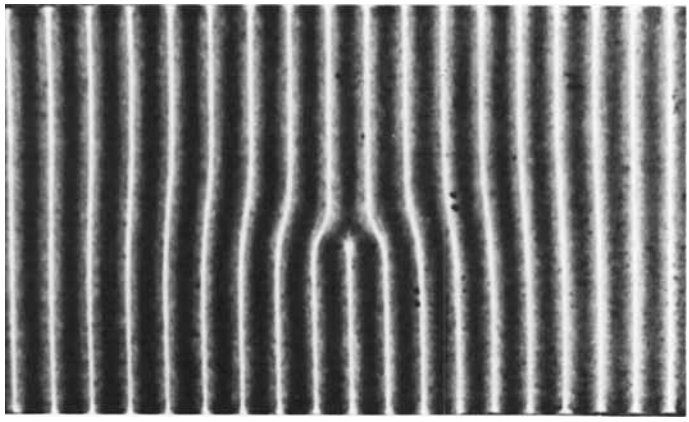

Figure 43. Induced structure of a roll pattern containing a dislocation. (Silicone oil $\nu = 0{\cdot}05$ stokes, $d = 2{\cdot}5$ mm, $a_1 = a_c$, $a_2 = (18/19)a_c$).

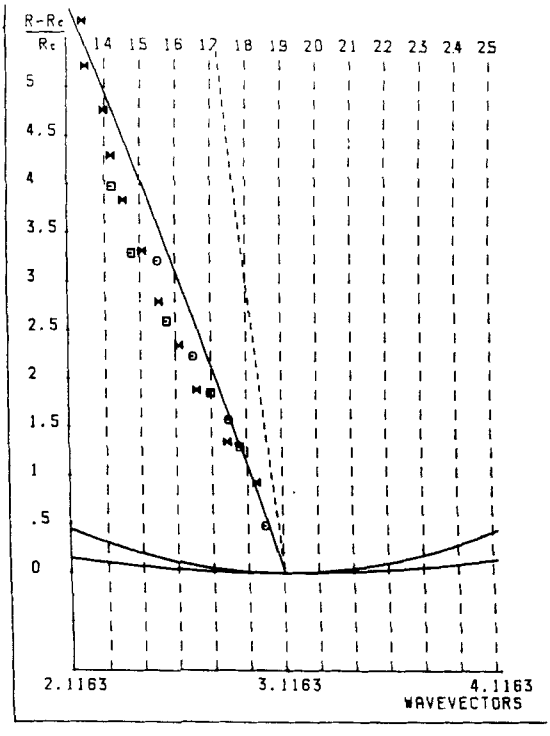

Figure 44. Experimental wavenumber selection compared to the $D_\perp = 0$ criterion ($Pr = 70$). The reported wavenumber is the arithmetic mean of the two wavenumbers of the structure. The circles correspond to zero dislocation velocity. The squares are the velocity zeros, deduced at a constant Ra number from the fit of the measured velocities V_D with the law $D_\perp^{3/2}$. The crosses correspond to the mean wavenumber of the central part of a structure such as that shown in figure 45 and thus give the wavenumber selection by grain boundaries. The full line and the dotted line are the computed curves $D_\perp = 0$, the full line being related to the case for which the secondary flows have been taken into account (see figure 42).

In an experimental device, where the number of rolls is finite, the structure under study (induced as described in section 3.2. and in figure 15) is in fact composed of two sets of rolls as shown in figure 43 with wavelengths L/N and $L/(N+2)$; L is the greatest extension of the layer, N is the number of rolls in one part and $N+2$ the number in the other part (N has been varied). These two sets of rolls are in phase right at the sidewalls and in phase opposition at the middle of the layer where the dislocation is produced.

The study of the evolution of such structures has revealed some important features (Pocheau and Croquette 1984).

(*a*) the dislocation always climbs and always favours the part of the structure with wavenumber closer to that corresponding to the condition $D_\perp = 0$ at the ε-value of the measurement (see figure 44).

(*b*) In the majority of the cases, the velocity of the dislocation V_D was uniform versus time. Its measured amplitude agrees reasonably with the expected relation

$$V_D \sim D_\perp^{3/2} \tag{47}$$

where $D_\perp$ is given by eqn. (46). Then V_D increases with the mean wavenumber of the structure and with the Rayleigh number; to give an order of magnitude, with silicone oil ($Pr = 70$) and $d \simeq 2{\cdot}5$ mm, $V_D = 0{\cdot}52$ cm/h at $\varepsilon = 1{\cdot}37$ and 5 cm/h at $\varepsilon = 4$ for a mean wavenumber $\langle a \rangle \simeq a_c$.

The line $V_D = 0$ in the plane, Ra, a corresponds to the 'optimal' wavenumber for the corresponding experiment and thus defines the wavenumber selection line which is equivalent in the present case to the condition $D_\perp \equiv 0$.

Another type of mechanism leading to a wavenumber selection has confirmed this universal criterion. If we look at a perfect roll structure in a rectangular box whose lateral part is ended by grain boundary defects as shown in figure 45, the two rows of lateral rolls enable the principal set of rolls to expand or to contract, so as freely to adjust its wavelength. The corresponding wavenumbers, measured as a function of the Rayleigh number lie on the curve $D_\perp = 0$ (see figure 44). (The conditions of the experiment were the same as those for the dislocation motions.)

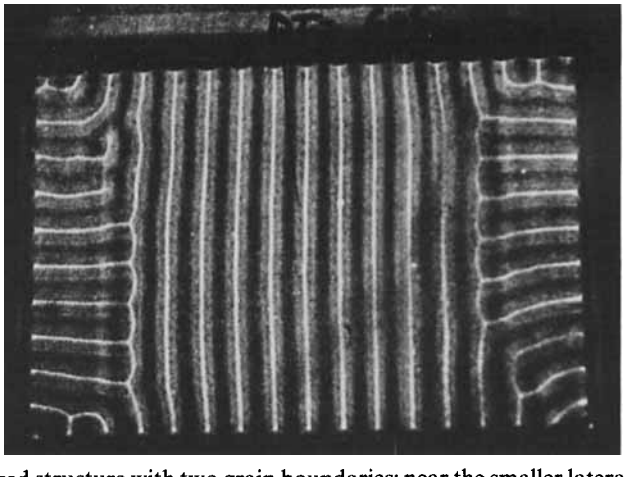

Figure 45. Induced structure with two grain boundaries: near the smaller lateral walls, two sets of rolls with axes perpendicular to those of the central part may expand or regress freely. (Silicone oil $\nu = 0{\cdot}05$ stokes, $d = 2{\cdot}56$ mm).

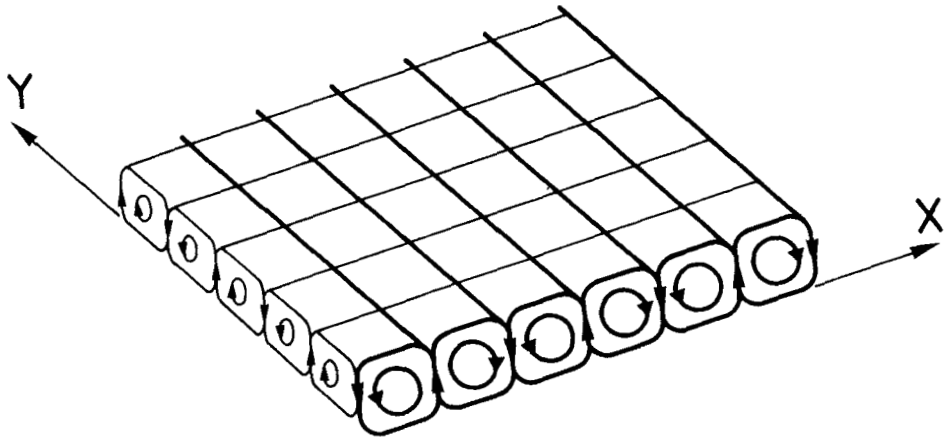

(*a*)

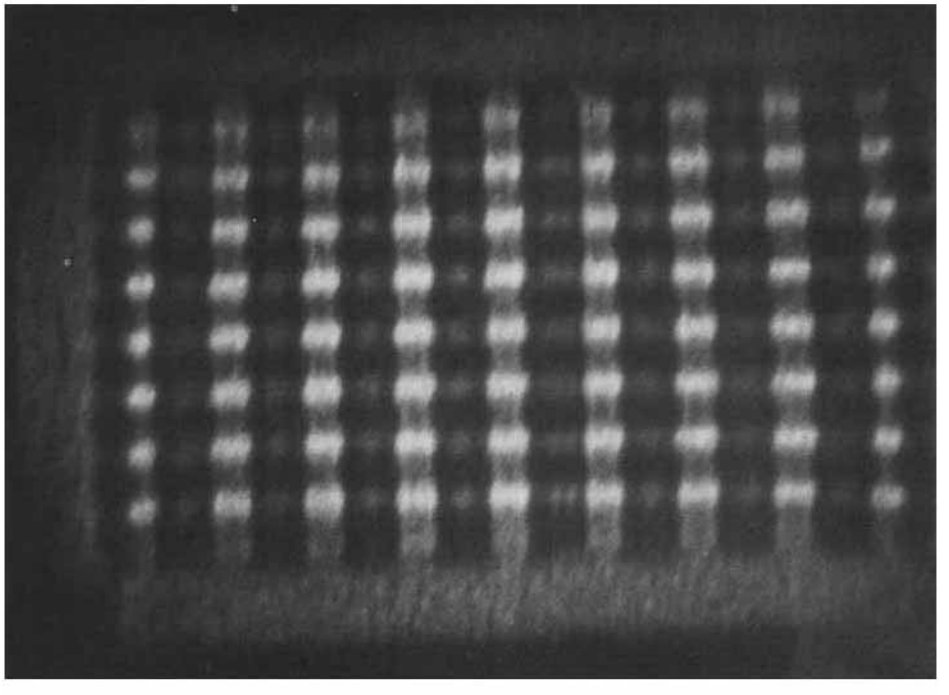

(*b*)

Figure 46. Three-dimensional convective structure. (*a*) Schematic representation of two perpendicular sets of rolls. (*b*) Photograph of a three dimensional pattern seen from above. (Silicone oil $\nu = 0{\cdot}1$ stokes, $d = 0{\cdot}5$ cm, $Ra \simeq 12\, Ra_c$). Notice the higher amplitude of the first set of rolls, as indicated by the large bright 'lines', in comparison with the less contrasted ones, which correspond to the new transverse set of rolls.

5.3. *Approach to turbulent states*

The field of Rayleigh–Bénard convection is so broad that the authors apologize for the long discussion so far concerning the properties near threshold. When the Rayleigh number is increased, other interesting phenomena appear, related to new bifurcations. We wish to mention here only their essential features.

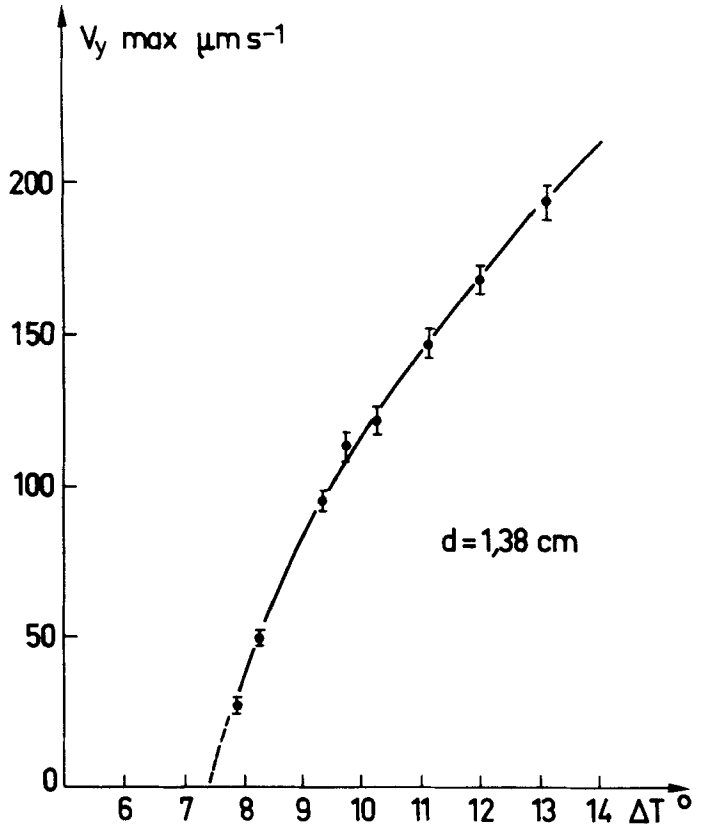

Figure 47. Appearance of the new component V_y of the velocity and dependence of its amplitude versus ΔT (Silicone oil $\nu = 1$ stokes, $\Delta T_c = 0°85$).

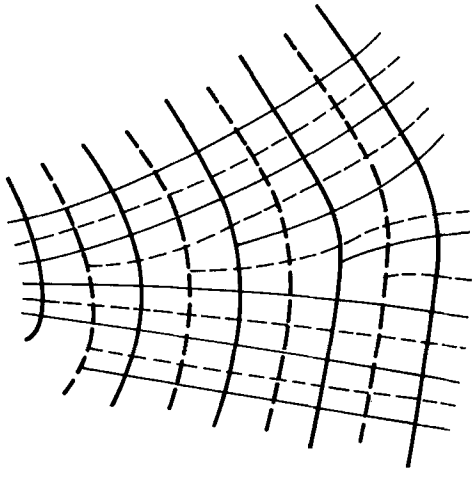

Figure 48. Topological frustration occurring when three-dimensional convection appears in an imperfect structure. This picture was obtained from a photograph (by 'shadowgraphic' technique) of a convective pattern at $Ra \simeq 10\, Ra_c$. Notice that, as the principal rolls (broad lines) are equidistant, the secondary rolls (thin lines) are variable in size and contain numerous dislocations (continuous lines: uprising streams; dashed lines: downgoing streams).

The first phenomenon is the appearance of three dimensional motion, whose spatial properties depend essentially on the Prandtl number. Recall that for small ε values, even if the velocity amplitude is dependent on x and y, the velocity field has only two components locally (except in the core of the defects), the horizontal one being perpendicular to the local roll axis. At a given value Ra_2, which depends on the Prandtl number and the geometry of the pattern, a new feature appears. For low Prandtl number fluids ($Pr<1$), an instability occurs in the form of transverse waves propagating along the rolls axes (Busse 1972). This oscillatory instability is time dependent.

For fluids with high Prandtl number ($Pr>10$), a new set of rolls appears, superimposed on the first rolls and such that the axes of the two sets of rolls are perpendicular (see figure 46), so the velocity must be described by three components (V_x, V_z and V_y). When this new set of rolls is added to a previously perfect structure (as shown in figure 13), the corresponding pattern is stationary. Then the amplitude $V_{y\max}$ of the new mode along the y direction varies in a manner similar to that of the first components V_x and V_z at the first bifurcation at Ra_c (see figure 47), i.e. as at a new second order phase transition (Bergé and Dubois 1978).

In disordered structures in high Pr fluids, the establishment of the new set of rolls leads to a new frustration. In fact, the new rolls have their own topological constraints: they have to be perpendicular to the first rolls and they must be arranged so as to define a new wavenumber a_y (see figure 48) in the whole pattern. In the case of the onset at Ra_c, the relaxation of the structure was able (by motion of defects) to release a large part of the topological constraints and therefore to reach an equilibrium state. However at this new bifurcation Ra_2, the complexity of the pattern makes such a relaxation no longer possible. As far as we know from a few observations (Bergé 1981, Gollub *et al.* 1982 a) a turbulent state is observed as soon as a disordered structure becomes three dimensional. This turbulence seems related to intermittent motion of the defects and rearrangement of the structure, which involve very long characteristic times (of the order of days in laboratory observations).

At higher value of the Rayleigh number, ordered and disordered structures exhibit more developed turbulence (Krishnamurti, 1970; Busse and Whitehead 1974).

Note that, in very small containers ($\Gamma_x \simeq 2, \Gamma_y \simeq 1$), where only a few rolls are present and where the influence of the lateral walls is dominant, spatial turbulence appears only at very high values of the Ra number ($Ra/Ra_c \simeq 400$ with $Pr \simeq 130$). So at intermediate Ra values periodic oscillatory regimes are observed and reliable observations in different fluids have clearly confirmed the existence of the deterministic chaos which is related to the presence of a small number of degrees of freedom. (Dubois 1982; Gollub and Benson 1980).

6. Conclusion

The Rayleigh–Bénard instability, i.e. the induction of motions in fluids submitted to destabilizing temperature gradients and related behaviour, are very common phenomena around us. Not only do these motions have considerable practical interest, for their transport properties and their time-dependent effects, but, in addition, the Rayleigh–Bénard instability has revealed itself to be a very rich system for the physicist. In fact, it provides a model system for different branches of physics. First of all, the instability exhibits phase-transition properties near threshold for which the critical exponents follow a mean field approach. Secondly, the spatial properties of the natural structures involve concepts of topological arrangement, frustration and motions of

defects as in crystals. Finally, convection at high *Ra* number is a particularly good system in which to study the approach to turbulence, introduced at first by the competition between spatial modes or the development of dynamical instabilities.

Acknowledgments

We want to thank especially V. Croquette and A. Pocheau for their contribution and in particular for many original results obtained from their experiments. Our acknowledgments also go to P. Manneville and L. Tuckerman for helpful discussions, Brigitte Valdés for careful typing and revision of the manuscript and B. Ozenda and C. Poitou for technical assistance.

Bibliography

AHLERS, G. 1974, *Physical Review Letters*, **33,** 1185.
AHLERS, G. and BEHRINGER, R. P., 1978, *Physical Review Letters*, **40,** 712.
BÉNARD, H., 1900, *Revue générale des sciences pures et appliquées*, **11,** 1261 and 1309.
BERGÉ, P., 1976, *Journal de Physique Colloque*, **C1,** 37, C1.
BERGÉ, P., 1981, *Chaos and order in nature*, edited by H. Haken (Springer-Verlag), p. 14.
BERGÉ, P., and DUBOIS, M., 1978, *Lecture notes in physics no. 72*, edited by J. C. Legros and J. K. Platten, p. 133.
BERGÉ, P., and DUBOIS, M., 1981, *Scattering techniques applied to supramolecular and non equilibrium systems*, edited by S. H. Chen, B. Chu and R. Nossal (Plenum publishing corporation), p. 493.
BÜHLER, K., KIRCHARTZ, K. R., and OERTEL, JR. H., 1979, *Acta Mechanica*, **31,** 155.
BUSSE, F. H., 1967 a, *Journal of Mathematics and Physics*, **46,** 140.
BUSSE, F. H., 1967 b, *Journal of Fluid Mechanics*, **30,** 625.
BUSSE, F. H., 1972, *Journal of Fluid Mechanics*, **52,** 97.
BUSSE, F. H., 1978, *Reports on Progress in Physics*, **41,** 1929.
BUSSE, F. H., and WHITEHEAD, J. A., 1971, *Journal of Fluid Mechanics*, **47,** 305.
BUSSE, F. H., and WHITEHEAD, J. A., 1974, *Journal of Fluid Mechanics*, **66,** 67.
CANNELL, D. S., DOMINGUEZ-LERMA, W. A., and AHLERS, G., 1983, *Physical Review Letters*, **50,** 1365.
CHEN, M. M., and WHITEHEAD, J. A., 1968, *Journal of Fluid Mechanics*, **31,** 1.
CROQUETTE, V., and SCHOSSELER, F., 1982, *Journal de Physique*, **43,** 1183.
CROQUETTE, V., MORY, M., and SCHOSSELER, F., 1983, *Journal de Physique*, **44,** 293.
CROSS, M. C., 1982, *Physical Review A*, **25,** 1065.
CROSS, M. C., 1983, *Physical Review*, A, **27,** 490.
CROSS, M. C., DANIELS, P. G., HOHENBERG, P. C., and SIGGIA, E. D., 1983, *Journal of Fluid Mechanics*, **127,** 155.
DUBOIS, M., and BERGÉ, P., 1978 a, *Journal of Fluid Mechanics*, **85,** 641.
DUBOIS, M., NORMAND, C., and BERGÉ, P., 1978 b, *International Journal of Heat and Mass Transfer*, **21,** 999.
DUBOIS, M., BERGÉ, P., and WESFREID, J., 1978 c, *Journal de Physique*, **39,** 1253.
DUBOIS, M., 1982, *Stability of thermodynamics systems*, edited by J. Casas-Vasquez and G. Lebon (Springer-Verlag), p. 177.
FARHADIEH, R., and TANKIN, R. S., 1974, *Journal of Fluid Mechanics*, **66,** 739.
FAUVE, S., LAROCHE, C., LIBCHABER, A., and PERRIN, B., 1984, *Lecture Notes in Physics*, edited by J. E. Wesfreid and S. Zaleski (Springer-Verlag) (to appear).
GOLLUB, J. P., and BENSON, S. V., 1980, *Journal of Fluid Mechanics*, **100,** 449.
GOLLUB, J. P., MCCARRIAR, A. R., and STEINMAN, J. F., 1982 a, *Journal of Fluid Mechanics*, **125,** 259.
GOLLUB, J. P., and MCCARRIAR, A. R., 1982 b, *Physical Review A*, **26,** 3470.
HOARD, C., ROBERTSON, C., and ACRIVOS, A., 1970, *International Journal of Heat and Mass Transfer*, **13,** 849.
KOSCHMIEDER, E. L., 1967, *Journal of Fluid Mechanics*, **30,** 9.
KOSCHMIEDER, E. L., and PALLAS, S. G., 1974, *International Journal of Heat and Mass Transfer*, **17,** 991.

KRISHNAMURTI, R., 1970, *Journal of Fluid Mechanics*, **42,** 295.
KRISHNAMURTI, R., 1975, *Journal of Atmospheric Sciences*, **32,** 1353.
MANNEVILLE, P., 1983, *Journal de Physique Lettres*, **44,** L903.
MANNEVILLE, P., and PIQUEMAL, J. M., 1983, *Physical Review A*, **28,** 1774.
NORMAND, C., POMEAU, Y., and VELARDE, M. G., 1977, *Review of Modern Physics*, **49,** 581.
PLATTEN, J. K., and LEGROS, J. C., 1983, *Convection in liquids* (Springer-Verlag).
POCHEAU, A., and CROQUETTE, V., 1984, *Journal de Physique*, **45,** 35.
POMEAU, Y., and MANNEVILLE, P., 1979, *Journal de Physique Lettres*, **40,** L609.
RAYLEIGH, LORD, 1916, *Philosophical Magazine*, **32,** 529.
SAWADA, Y., 1978, *Physics Letters*, **65A,** 5.
SOMERSCALES, E., and DOUGHERTY, T. S., 1970, *Journal of Fluid Mechanics*, **42,** 755.
STORK, K., and MÜLLER, U., 1972, *Journal of Fluid Mechanics*, **54,** 599.
STORK, K., and MÜLLER, U., 1975, *Journal of Fluid Mechanics*, **71,** 231.
THOMSON, J., 1881–82, *Proceedings Glasgow Philosophical Society.*
VELARDE, M. G., 1973, *Fluid Dynamics, Cours des Houches*, edited by Balian and Peube (Gordon and Breach Science Publishers), p. 473.
WESFREID, J. E., POMEAU, Y., DUBOIS, M., NORMAND, C., and BERGÉ, P., 1978, *Journal de Physique*, **39,** 725.
WESFREID, J. E., BERGÉ, P., and DUBOIS, M., 1979, *Physical Review A*, **19,** 1231.
WESFREID, J. E., and ZALESKI, S., 1984, *Cellular structures in instabilities, Lecture notes in Physics* (Springer-Verlag), (to appear).
ZAMORA, M., and REY DE LUNA, A., 1984, *Cellular structures in instabilities*, edited by J. E. Wesfreid and S. Zaleski (Springer-Verlag), (to appear).
ZIEREP, J., and OERTEL, H., 1982, *Convective transport and instability phenomena* (G. Braun Karlsruhe).